International Journal of Greenhouse Gas Control 136 (2024) 104175

Contents lists available at ScienceDirect

International Journal of Greenhouse Gas Control

journal homepage: www.elsevier.com/locate/ijggc

CO_2 storage potential of the Middle Buntsandstein Subgroup - German sector of the North Sea

A. Fuhrmann *, S. Knopf, H. Thöle, F. Kästner, N. Ahlrichs, H.L. Stück, A. Schlieder-Kowitz, G. Kuhlmann

Federal Institute for Geosciences and Natural Resources (BGR), Hanover, Germany

ARTICLE INFO

Keywords:
CO_2 storage capacity
Carbon capture and storage (CCS)
Buntsandstein
German North Sea
Reservoir evaluation
Saline aquifers

ABSTRACT

The storage of CO_2 in deeply buried geological formations provides a contribution to mitigate hard-to-abate CO_2 emissions from industry. Robust geological models and capacity estimations are crucial for the successful planning and implementation of safe storage projects. This study focuses on the CO_2 storage potential of the Middle Buntsandstein Subgroup within the Exclusive Economic Zone of the German North Sea. We have mapped a total of 71 potential storage sites based on existing 3D models, seismic and well data. Static CO_2 capacities are calculated for each structure using Monte Carlo simulations with 10,000 iterations to account for uncertainties. All potential reservoirs are evaluated based on their potential capacity, burial depth, top seal integrity and trap type. We have identified 38 potential storage sites with burial depths between 800 m and 4500 m, reservoir capacities (P50) above 5 Mt CO_2 and suitable sealing units. The estimated cumulative static storage capacity percentiles of these structures range between P10 = 902.08 Mt and P90 = 5508.93 Mt, with P50 = 2554.10 Mt. We expect the best storage conditions on the West Schleswig Block, where salt-controlled anticlines with moderate burial depths, large reservoir capacities and limited lateral flow barriers are the dominant trap types. Relatively poor storage conditions can be expected for small (P50 < 5 Mt CO_2), deeply buried (> 4500 m) and structurally complex potential storage sites in the Horn and Central Graben. Our study highlights the most prolific reservoirs and discusses the most suitable locations for further exploration.

1. Introduction

Carbon dioxide removal from the atmosphere and capture from industrial sources is considered an important tool to mitigate human made climate change and reach the 1.5 °C goal of the Paris agreement (IPCC, 2018). One technology is the capturing of carbon dioxide (CO_2) and its sequestration in deeply buried geological formations, widely known as Carbon Capture and Storage (CCS). Despite the availability of the technology, and its potential to counterbalance the hard-to-abate residual emissions from industry, the development of large-scale CCS projects has been slow over the past decade (Martin-Roberts et al., 2021). The implementation of large-scale CCS projects depend on a good coordination between policy makers and industry stakeholders, technology development in terms of CO_2 capture, development of monitoring technologies as well as robust geological models to plan and implement safe subsurface storage of CO_2 (Celia, 2017; Damen et al., 2009).

The North Sea has become one of the most promising locations for CO_2 storage in Europe due to its extensive regions with promising geology, data availability, and existing infrastructure. Several studies investigated the CO_2 storage potential for Denmark, the Netherlands, Norway and the UK showing high storage potential in a variety of geological settings in abandoned hydrocarbon fields and saline aquifers (Anthonsen et al., 2014; 2016; Bentham et al., 2014; Halland et al., 2013; Holloway et al., 2006; Lloyd et al., 2021a). In contrast to the well-studied hydrocarbon provinces of its neighbours, the German sector of the North Sea remains relatively understudied with sparse data in terms of modern 3D seismic and available well data. Understanding the storage potential of this region is crucial for expanding CCS options in the German North Sea. Initial screening work in this area focussed on the identification of trap types and the distribution of potential reservoir and seal units for potential carbon dioxide storage sites (Bense and Jähne-Klingberg, 2017). The authors indicated that the Middle Buntsandstein Subgroup is the most prolific target for large-scale CO_2 storage

* Corresponding author.
E-mail address: arne.fuhrmann@zohomail.eu (A. Fuhrmann).

https://doi.org/10.1016/j.ijggc.2024.104175
Received 16 April 2024; Received in revised form 24 May 2024; Accepted 8 June 2024
Available online 16 July 2024

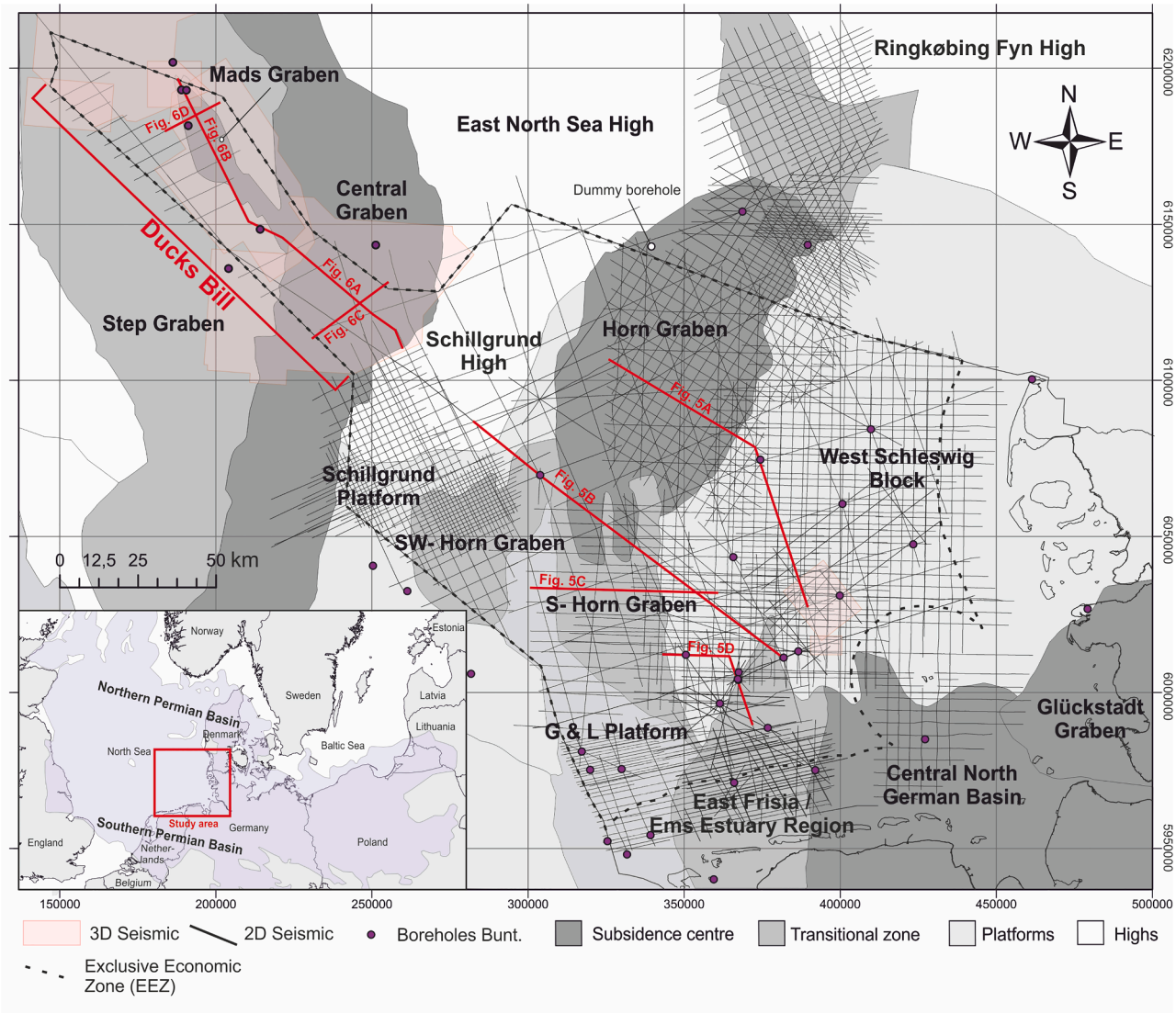

Fig. 1. Map showing the study area including used 2D and 3D seismic reflection data and wells that target the Middle Buntsandstein Subgroup. Structural elements after Thöle et al. (2021).

developments offering lateral continuous reservoir and seal facies. First estimates of the static storage potential onshore and offshore Germany do not cover the entirety of the German North Sea (Knopf and May, 2017; Vangkilde-Pedersen et al., 2009). Such capacity estimates need further evaluation in terms of geological setting, preliminary storage safety assessments, and ranking in terms of geotechnical feasibility (Lloyd et al., 2021b).

Our study aims to comprehensively assess the static CO_2 storage potential of the Middle Buntsandstein Subgroup in the German North Sea EEZ, utilizing existing geological data and a Monte Carlo simulation approach. We further map faults in the main sealing units and discuss the most prolific targets for further exploration and detailed reservoir modelling.

2. Geological setting

2.1. Tectonic history

The area of work is located within the Southern Permian Basin, which covers large parts of Central Europe (Fig. 1). This intra-cratonic basin was formed in latest Carboniferous and Early Permian times after a wrench induced collapse of the Variscan mountain belt in response to a dextral translation between Africa and Europe during the break up of Pangea (Pharaoh et al., 2010; Ziegler, 1990). Extensive volcanism, thermal doming and erosional thinning of the crust was followed by thermal subsidence of the basin in the Early Permian that controlled the basin dynamics until the Mid-Triassic (Bachmann and Hoffmann, 1997; van Wees et al., 2000; Wilson et al., 2004). Subsidence outpaced sedimentation in the Late Permian and the basin was flooded by the Arctic Sea causing the deposition of thick evaporitic successions of the Zechstein (Fig. 2) (Geluk, 2005; Tucker, 1991). East-west orientated rifting related to southward propagation of the Arctic-North Atlantic rift system in the Triassic controlled the accelerated subsidence of the Central, Horn and Glückstadt Graben (Kley et al., 2008; Pharaoh et al., 2010). The latter ones were dominantly active during the Early Triassic and show major syn-depositional thickness increase during the deposition of the Buntsandstein succession (Kilhams et al., 2018; Röhling, 1991). Salt movements initiated pillow build-up in the Middle to Late Triassic with piercing salt domes and rim-synclines developed during Triassic, Jurassic, Late Cretaceous or Cenozoic times, varying locally in the basin (Fig. 2) (Buchanan et al., 1996; Mohr et al., 2005; Warsitzka et al., 2018). Rifting persisted until the Mid-Jurassic when crustal separation of the Central Atlantic Rift and the opening of the Tethys Ocean caused a reorientation of the stress field (Fig. 2) (Pharaoh

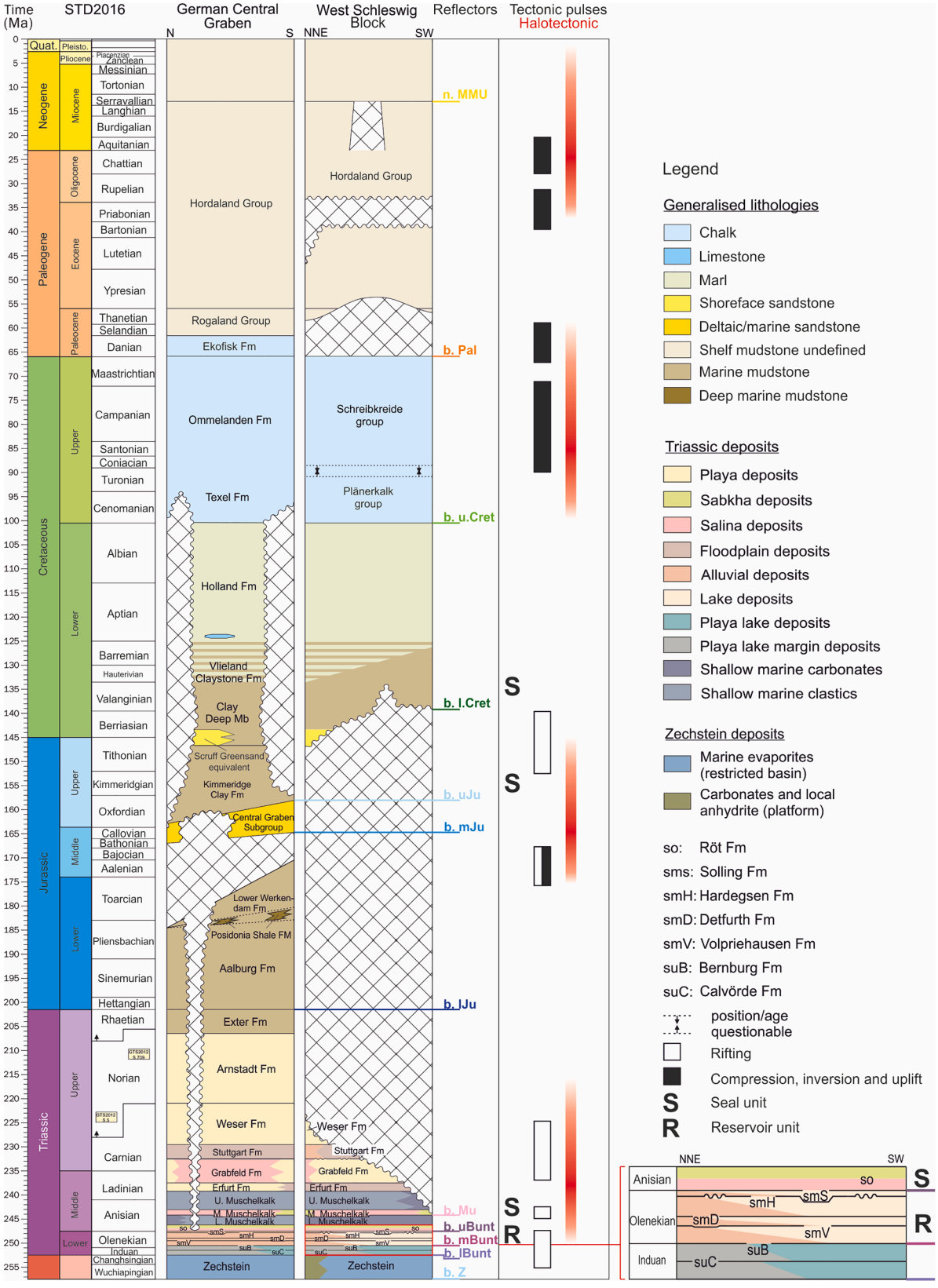

Fig. 2. Stratigraphic column of the German North Sea with a focus on the West Schleswig Block and the Central Graben including the stratigraphic framework and seismic reflectors (after Thöle et al., 2020). The generalised tectonic events are adapted from Warsitzka et al. (2018) and Pharaoh et al. (2010).

et al., 2010). Thermal doming and uplift in the Central North Sea caused deep erosion into Lower Jurassic and Triassic strata and development of the Cimmerian Unconformity (Fig. 2) (Pharaoh et al., 2010; Underhill and Partington, 1993). Rifting along the Jurassic-Cretaceous transition caused the development of transtensional basins (Ziegler, 1990). This stress induced uplift in combination with an eustatic sea-level low stand lead to widespread erosion in the area of the Southern Permian Basin and a basin-wide unconformity complex – often referred to as 'base Cretaceous' or 'late Cimmerian' unconformity (Fig. 2) (Kyrkjebø et al., 2022; Pharaoh et al., 2010). A subsequent phase of thermal subsidence and sea-level rise in the Late Cretaceous caused extensive transgression, flooding of the Southern Permian Basin and the deposition of thick chalk deposits (Pharaoh et al., 2010; van der Molen et al., 2005). North-east-orientated stresses occurred due to the counter-clockwise rotational convergence of Africa-Iberia with Europe during the closure of the Tethys and the Alpine Orogeny (Fig. 2) (de Jager, 2003; Dèzes et al., 2004; Kley, 2018; Kley and Voigt, 2008). Decoupling effects of the Zechstein salt caused locally variable inversion and fault reactivation patterns in the southern North Sea (Kley and Voigt, 2008). The Cenozoic is characterised by subsidence in the North Sea thermal sag basin (Kley et al., 2008; Ziegler, 1990).

2.2. Stratigraphy

Triassic sediments of the Buntsandstein, Keuper and Muschelkalk and their equivalents conformably overly the sabkha-dominated upper Zechstein deposits (Fig. 2) (Ziegler, 1990). The Buntsandstein Group was deposited under semi-arid conditions in the almost completely landlocked Southern Permian Basin, which was located between 20° and 30° N (Bachmann et al., 2010). Sedimentation was controlled by wet-dry cycles and tectonic pulses (Geluk and Röhling, 1997; McKie and Williams, 2009). The Lower Buntsandstein consists of fine-grained playa lake deposits in the basin centre and alluvial and fluvial sedimentary systems that were restricted to the basin margins (Fig. 2) (Röhling, 1991). Individual tectonic pulses in the Olenekian controlled sedimentation, created topography along swells and enhanced subsidence along the Horn, Gückstadt and Central Graben (Bachmann et al., 2010; Ziegler, 1990). The four tectonostratigraphic units of the Middle Buntsandstein Subgroup (Volpriehausen, Detfurth, Hardegsen, and Solling Formations) are associated with these individual tectonic pulses (Fig. 2) (Geluk and Röhling, 1997). The pre-Solling pulse was the strongest and caused the extensive Hardegsen Unconformity (Fig. 2) (Röhling, 1991). Erosional bases are overlain by aeolian- and fluvial sandstones that grade into thin-bedded silt- and mudstones deposited in a playa lake environment (Olivarius et al., 2015). Sediment was sourced from the Variscan massive in the south and the Mid-North Sea High and Ringkøbing Fyn High in the north (Fig. 1) (Bourquin et al., 2009; Kortekaas et al., 2018; Olivarius et al., 2017). Sediment transport was dominated by river systems during wet periods and reworked by aeolian processes during dry periods (McKie and Williams, 2009; Olivarius et al., 2017). Aeolian processes decrease towards the top of the succession, except for local depocentres and syn-sedimantary faulting (de Jager, 2014). The overlying Röt Formation of the Upper Buntsandstein is deposited in a sabkha environment and mainly consists of evaporites, red marls, and clay deposits (Fig. 2) (Bachmann et al., 2010). A major transgression of the Tethys from the southwest in Anisian times caused the deposition of shallow marine carbonates of the Muschelkalk sequence (Fig. 2) (Geluk, 2005). During the Ladinian and Rhaetian, the Southern Permian Basin was dominated by deltaic, hypersaline and non-marine deposits of the Keuper Group (Fig. 2) (Bachmann et al., 2010). Most of the Jurassic stratigraphy is missing due to deep incision by the Middle and Late Jurassic unconformities, except for parts of the Central and Step Graben (Fig. 2) (Arfai et al., 2014; Kyrkjebø et al., 2022; Müller et al., 2023). Here, Jurassic deposits mainly consist of marine mudstones and locally developed fluvial-deltaic deposits of the Central Graben Subgroup and shallow marine sandstones of the Scruff Greensand equivalents (Fig. 2) (Bouroullec et al., 2018; Michelsen et al., 2003). Elsewhere, Triassic sediments are unconformably overlain by marine mudstones of the Lower Cretaceous and Chalk deposits of the Upper Cretaceous (Fig. 2) (van der Molen, 2004).

2.3. CO_2 reservoir and seal formations

Triassic sandstones of the Middle Buntsandstein Subgroup are prolific reservoir rocks that have been investigated for decades (Bachmann et al., 2010; Geluk et al., 2018; Kortekaas et al., 2018). Fluvio-aeolian sandstones at the base of the Volpriehausen, Detfurth and Solling Formations are well-correlated across the basin, with local depocentres along swells and syn-sedimentary faulting may control local reservoir distribution and quality (de Jager, 2014; Fontaine et al., 1993; Olivarius et al., 2015). Sandstones of the Solling Formation may form prolific reservoir rocks along basin margin and within local depocentres (de Jager, 2014; Olivarius et al., 2017). Reworked aeolian sandstones tend to have the best reservoir properties and, with some exceptions, are dominant along the basin margins and the lower part of the Buntsandstein Group (Olivarius et al., 2017, 2015). However, in-situ porosity and permeability data of the Buntsandstein Group from the German North Sea are sparse, as most past exploration data were gathered onshore or different stratigraphic intervals (Dethlefsen et al., 2014). Exploration data from the Netherlands provide a suitable distribution of porosity values over a large depth interval (down to 4500 m) for a regional assessment (NLOG, 2023; van Kempen et al., 2018). A reservoir thickness of 10 m is considered suitable for potential CO_2 storage (Bense and Jähne-Klingberg, 2017; Müller and Reinhold, 2011). A suitable seal with capillary entry pressures well above the injection pressures and a minimum thickness of 20 m is provided by claystone and evaporites (Bense and Jähne-Klingberg, 2017; Chadwick et al., 2008; Müller and Reinhold, 2011). The most important seal for the Buntsandstein Subgroup in the Dutch and German sectors are the evaporites and mudstones of the Upper Buntsandstein (Fig. 2) (Bense and Jähne-Klingberg, 2017; Kilhams et al., 2018). Mudstones of the Solling Formation act as a sealing unit in parts of the Netherlands, but may only contribute locally towards seal thickness in the German sector of the North Sea (Fontaine et al., 1993). The silt-prone interbedded facies between the reservoir units of Volpriehausen, Detfurth and Hardegsen may act as local barriers, but do not represent reliable regional seal formations (Fig. 2) (Korevaar et al., 2023). In the Central and Mads Graben area (Fig. 1), as well as in areas where the Upper Buntsandstein seal is partly eroded, marine mudstones of the Upper Jurassic and Lower Cretaceous act as important seal formations (Müller et al., 2023).

3. Data and methods

3.1. Data and reservoir mapping

The stratigraphic framework and horizons are based on existing 3D models that cover the Ducks Bill (DB) and the Central German North Sea (CNS) (Thöle et al., 2022, 2020; Wolf et al., 2015) (Fig. 1 & 2). Additionally, we use available 2D and 3D seismic reflection data of different vintages and varying resolution for local reinterpretations and horizon gridding around individual potential storage sites (Data Repository - DR. 1). Seismic data and existing 3D models were loaded in Aspen EPOS™ and SeisEarth applications, shifted according to a common datum to allow for coherent interpretation. The seismic data are displayed in zero phase, with European polarity, where an increase in acoustic impedance is represented by a trough (Brown, 2001). A time-to-depth conversion was performed using regional velocity models for the Ducks Bill (Doornenbal et al., 2021) and the Central German North Sea (Bense et al., 2022). Individual trap structures are mapped along 50 m spaced contour lines along the top reservoir surface to identify local spill points. The top seal of sandstone reservoirs in the Middle Buntsandstein Subgroup is represented by the base of Upper Buntsandstein, the first

regional sealing unit. In areas where this top seal is eroded, the base of the Upper Jurassic or Lower Cretaceous was defined as the top reservoir unit. The reservoir top surface and polygons delimiting individual reservoir structures are loaded in ArcGIS Pro, where each polygon is attributed according to its location, trap type, depth (top and base), net-sandstone thickness and porosity. For the potential reservoir thickness all sandstone beds above one metre thickness are considered within the Middle Buntsandstein Subgroup. This net-sandstone thickness was taken from well reports and log data of 39 former exploration wells and correlated using the Spline tool in ArcGIS Pro (DR. 1). Data availability varies greatly throughout the area of work with no wells penetrating the Middle Buntsandstein Subgroup in the Horn and Central Graben and sparse data in the Ducks Bill. Additional wells were added along the Dutch and Danish borders to support the thickness estimation (Fig. 1). The long correlation distances between some of the wells may cause increased uncertainties compared to wells just a few kilometres apart. These uncertainties can be accepted locally due to little thickness variability apparent in seismic data and the lateral continuous nature of the Middle Buntsandstein sedimentary systems. Unreasonably high net-sandstone thickness values occurred towards the Danish sector on the north-eastern shoulder of the Horn Graben, where values exceeded the overall thickness of the Middle Buntsandstein Subgroup. A dummy well was added on the north-eastern shoulder of the Horn Graben mirroring reasonably values from the other side of the Graben with similar seismic thicknesses of the Middle Buntsandstein Subgroup (Fig. 1).

3.2. Parameterisation and capacity calculation

We performed Monte Carlo simulations with 10,000 iterations for each mapped structure to derive the probability distribution of static CO_2 storage capacity as follows:

$$K = A \cdot M \cdot \Phi \cdot \rho_{CO_2} \cdot SE \quad (1)$$

Given the data availability, we focus on structural trapping where the migration of supercritical CO_2 in the reservoir along buoyancy and pressure gradients is mitigated by a suitable seal (*sensu* Chadwick et al., 2008). The calculation is based on Eq. (1), where each parameter is given an individual error distribution according to the available data and uncertainty; K is the effective storage capacity; A = area of the reservoir; M = reservoir net thickness; ϕ = average porosity; ρ_{CO_2} = density of CO_2; SE = storage efficiency factor. We used the software "Grapher" (Version 11.0.659) by Golden Software Inc. to perform spreadsheet-based Monte Carlo simulations. Built-in functions "*randn(x, y)*", to generate normally distributed real random numbers with mean x and standard deviation y, and "*randu(x)*", to generate uniformly distributed real random numbers from the interval [0, x], were used to generate probability distributions for the input parameters (each parameter with 10,000 values). For the parameters area (A), net thickness (M), and CO_2 density (ρ_{CO_2}) we assumed a normal distribution with a given mean and standard deviation, whereas for storage efficiency (SE) we assumed uniform distribution.

The area and average thickness for each individual reservoir is calculated using the Zonal Statistic Tool in ArcGIS PRO for the appropriate raster. The input data in terms of area, thickness and depth for each potential storage site are given in DR. 2. The data distribution was taken according to the standard deviation of the raster data and additional +/−5 % to honour the uncertainty of the underlying 3D models and seismic data. In-situ porosity data are not available for the Middle Buntsandstein in most areas of the German North Sea. We used publicly available porosity data of the Middle Buntsandstein from the Netherlands (NLOG, 2023; van Kempen et al., 2018). This analogue is suitable due to the well-established stratigraphic correlation and lateral homogenous facies distribution of the Middle Buntsandstein Subgroup (Bachmann et al., 2010; Geluk and Röhling, 1997; Kortekaas et al., 2018). We filtered the data according to the minimum and maximum formation depth providing analogue porosity samples at each individual storage site. For each sample histogram, we performed a random variate sampling with 10,000 random samples that represents a matching likelihood distribution for each depth interval (DR. 3). For the above calculations, we used python (3.10.2) and the scipy (1.8.1) functions *rv_histogram()* and *rvs()*. The latter deploys a uniform random number generator (MT19937 bit generator, seed=2409) and performs an inverse transform sampling method for the random variate sampling (Baumgarten and Patel, 2022).

Due to the lack of site specific and regional pressure and temperature data in the deep subsurface, we were not able to calculate site-specific CO_2 densities. To provide reasonable estimates, we calculated average CO_2 density values for the target depth interval below 800 m. We considered an average hydrostatic pressure gradient of 10 MPa/km and an average temperature gradient of 30 K/km and applied a formula by Span and Wagner (1996) to calculate CO_2 densities for the average depth interval (average min., average mean, average max.) of all mapped reservoir structures below 800 m. The resulting densities of the supercritical CO_2 did not vary much within the considered depth range and averaged at ca. 0.67 t/m^3. A standard deviation of 0.05 t/m^3 was chosen to reflect effects of assumed temperature gradient variations (25 – 35 K/km) on the density.

The storage efficiency factor, i.e., the amount of CO_2 effectively stored in the available pore space, depends on several factors such as facies variability, trap type and lateral connectivity of the reservoir (e.g., anticline versus four way structural closure) (Chadwick et al., 2008). In addition to reservoir characteristics, storage efficiency is also depending on factors concerning storage operation schemes or regulatory constraints (Bachu, 2015). We have applied a range of 5 % to 20 % for the storage efficiency factor to account for a large variability of trap types encountered in this study and uncertainties regarding porosity and permeability distribution. This range is in accordance with other regional static CO_2 storage estimates, which makes comparison across borders possible (Knopf and May, 2017; Vangkilde-Pedersen et al., 2009). We chose a uniform distribution for the storage efficiency factor in the Monte Carlo simulations, due to limited data and resulting inability to predict the probability range of the efficiency value for each storage site.

3.3. Structural complexity and fault analysis

Structural complexity plays an important role for CO_2 storage in saline aquifers due to its influence on injection pressure, lateral migration of pore fluids within the reservoir, into adjacent hydraulic units, or potential leakage pathways along faults (Birkholzer et al., 2015; Rutqvist, 2012). Although faults may not necessarily pose a risk in terms of their sealing capacity and reactivation potential, it is indispensable to evaluate their location, hydraulic properties, and geometrical complexity, if sites should be characterized for potential CO_2 storage. The higher the anticipated structural complexity of a screened area is, the greater the efforts for site characterization have to be and the larger the uncertainties will be in further safety assessments. Overall project risks tend to be larger in structurally complex regions compared to tectonically simpler settings. Hence, in a site screening phase, a structural analysis can be helpful for a preliminary site ranking. According to the regional scale of our work, we mapped major fault systems that are in connection with the top seal and potentially the seabed. We used the fault planes of the TUNB Model (Thöle et al., 2022) to calculate lineaments along fault intersections and the intersections with key horizons such as the top reservoir, polygonal fault systems along the Mid Miocene Unconformity (MMU) and seafloor (depth plus 100 m due to poor seismic resolution at shallow intervals) (Fig. 2). With this information, we are able to differentiate between five classes of faults in the overburden of potential storage formations: Class 1 - Faults from the top of the reservoir reaching near the seafloor with large displacement and potential lateral connection to non-sealing units; Class 2 - Faults from

the top of the reservoir to the seafloor with minor displacement; Class 3 – Faults in the seal with potential connection to the polygonal fault system; Class 4 - Minor faults in the seal; Class 5 - No faults. Additionally, we qualitatively discuss the distribution of salt diapirs and pillows that may form lateral barriers and complicate fluid migration and pressure dissipation. A potential lateral confinement or baffle is assumed if a displacing fault or salt diapir is present within 5 km distance to the potential storage site. Other causes for confinement are erosive unconformities (i.e., erosion or pinch out of the reservoir) or if a structural domain is isolated from the rest of the reservoir formation, such as in a graben setting. The attributes "unconfined" without barriers or baffles, "semi-confined" with one or more sides blocked by a barrier and "confined" with all sides potentially blocked for fluid migration are assigned to each potential storage sites (DR. 2 & Table 1). These description are used to discuss the lateral confinement of individual potential storage sites in certain tectonic domains and identify the most suitable target area for future exploration.

4. Results

4.1. Middle Buntsandstein reservoir mapping, net-sandstone and seal thickness

We mapped individual trap structures along the base surface of the Upper Buntsandstein and the base of the Lower Cretaceous where it is directly overlying the potential reservoir unit of the Middle Buntsandstein Subgroup (Fig. 3A & DR3). The net-sandstone thickness map based on the 39 former exploration wells is shown in Fig. 3B. Net-sandstone thicknesses in the Ducks Bill are relatively constant with average values around 85 m in the southwest and up to 140 m in the north, in the Mads Graben (Fig. 3B). Maximum net-sandstone thickness in the central part of the German North Sea are reached in the Horn Graben with up to 210 m close to the Danish border. Thicknesses gradually decrease in the southern and south-western branches of the Horn Graben down to 120 m and 80 m, respectively. The net-sandstone thickness on the West Schleswig Block decrease from 120 m in the southwest to 35 m in the northeast of this tectonic domain. Local minima are encountered in the East Frisia – Ems Estuary Region with 30 m and along the G&L Platform with only 20 m.

The Middle Buntsandstein is absent or eroded along the Schillgrund High, G&L Platform, the inverted Mads Graben and locally along salt diapirs and uplifted salt pillows. The main seal unit for the aquifers of the Middle Buntsandstein Subgroup in the EEZ of the German North Sea are the Upper Buntsandstein and Lower Cretaceous (Fig. 2 & 4). The evaporites and mudstones of the Upper Buntsandstein are continuously overlaying the Middle Buntsandstein aquifers with a suitable thickness. It reaches thicknesses of 170 m in the Mads Graben and gradually thickens to 1200 m in the Central Graben (Fig. 4A). In the central part of the German North Sea, the Upper Buntsandstein reaches its maximum thicknesses of 1400 m in the Horn Graben, thinning towards the southern and south-eastern branches. Its thickness across the West Schleswig Block remains relatively constant at about 200 m (Fig. 4A). Regional erosive unconformities and local erosion above salt pillows and diapirs can disrupt the seal continuity of the Upper Buntsandstein (Fig. 3A, 4A & 5). Extensive erosion occurred along the Mads Graben where dipping Triassic strata is overlain by Upper Jurassic mudstones along the west shoulder forming a stratigraphic trap (Fig. 6B & D). Large scale erosion also occurs along the Schillgrund High and the G&L Platform where Lower Cretaceous mudstones act as the main seal (Figs. 3A, 4B & 5B). Smaller erosive events along the Horn Graben during the Keuper caused erosion of the Upper Buntsandstein that decreases the seal thickness below 20 m in CNS_17 (Fig. 4A). Complete or partial erosion of the Upper Buntsandstein seal is also common above salt diapirs along the Horn Graben and above salt pillows on the West Schleswig Block (Fig. 5). Along these erosive contacts, the Upper Buntsandstein and Lower Cretaceous marine mudstones can form compound top seals to reach the minimum thickness of 20 m such as in CNS_24 (Fig. 5D). The marine mudstones of the Lower Cretaceous show varying thicknesses up to 800 m in the north of the Ducks Bill and Central German North Sea. It is widely eroded across the Ducks Bill where it is absent along the Mads High, Step Graben and can only locally contribute as a seal for underlying aquifers. In the Central German North

Table 1
The 20 largest potential CO_2 storage sites based on their P50 percentiles.

Lead No.	Trap type	Tectonic area	Fault class	Confinement (sides)	Well penetration	Area [km²]	Thickness (m)	Apex depth (m)	P10 (Mt)	P50 (Mt)	P90 (Mt)
CNS_20	salt-strat	Horn Graben S	1	confined (3)	0	388.13	119.13	692.81	152.84	562.43	1164.29
CNS_13	salt	Horn Graben	2	confined (3)	0	302.52	157.35	1900.00	119.07	383.51	891.76
CNS_24	anticline	West Schleswig Block	2	open	1	251.12	97.98	1181.07	159.59	368.11	685.70
CNS_9	salt-strat	Horn Graben	5	confined (3)	0	323.30	118.14	1798.79	103.67	314.83	733.53
CNS_34	anticline-salt	West Schleswig Block	2	semi-confined (2)	1	283.12	59.33	905.40	80.36	220.41	440.12
CNS_19	salt-strat	West Schleswig Block	1	open	1	207.70	74.59	424.05	72.49	204.26	396.77
CNS_6	salt-strat	Horn Graben SW	5	confined (4)	1	243.62	99.25	1833.42	72.09	200.53	459.56
CNS_32	anticline-fault	West Schleswig Block	1	semi-confined (1)	0	116.03	80.29	777.64	45.01	124.23	240.38
CNS_7	salt	G&L-Plattform	5	confined (4)	0	117.03	81.03	1370.31	30.16	88.13	207.23
CNS_4	anticline-strat	Horn Graben SW	5	confined (4)	0	104.51	87.63	2324.61	28.92	83.84	184.64
CNS_18	anticline	West Schleswig Block	4	open	0	140.71	61.47	1674.17	25.02	83.37	186.30
CNS_17	salt	Horn Graben	5	confined (3)	0	59.22	170.84	3201.70	20.46	76.94	178.40
CNS_33	anticline	West Schleswig Block	5	open	1	203.15	50.94	1809.48	26.11	72.62	191.00
CNS_16	fault	Horn Graben	3	confined (3)	0	46.43	186.64	2813.20	21.83	68.99	161.32
CNS_26	anticline	West Schleswig Block	5	open	1	74.50	67.48	1417.02	24.47	66.33	127.47
CNS_22	strat	G&L Plattform	5	semi-confined (2)	1	90.45	46.84	1371.77	25.52	61.24	114.13
DB_15	salt-fault	Central Graben	3	confined (3)	0	79.66	83.84	3550.61	12.86	51.05	116.24
CNS_15	anticline	Horn Graben	5	semi-confined (2)	0	83.85	82.06	2125.73	12.52	43.59	125.26
DB_2	fault-strat	Mads Graben	3	confined (4)	0	60.72	85.41	2619.12	15.10	43.16	99.77
DB_28	anticline	West Schleswig Block	5	open	0	72.01	56.77	1736.90	11.18	35.98	83.22

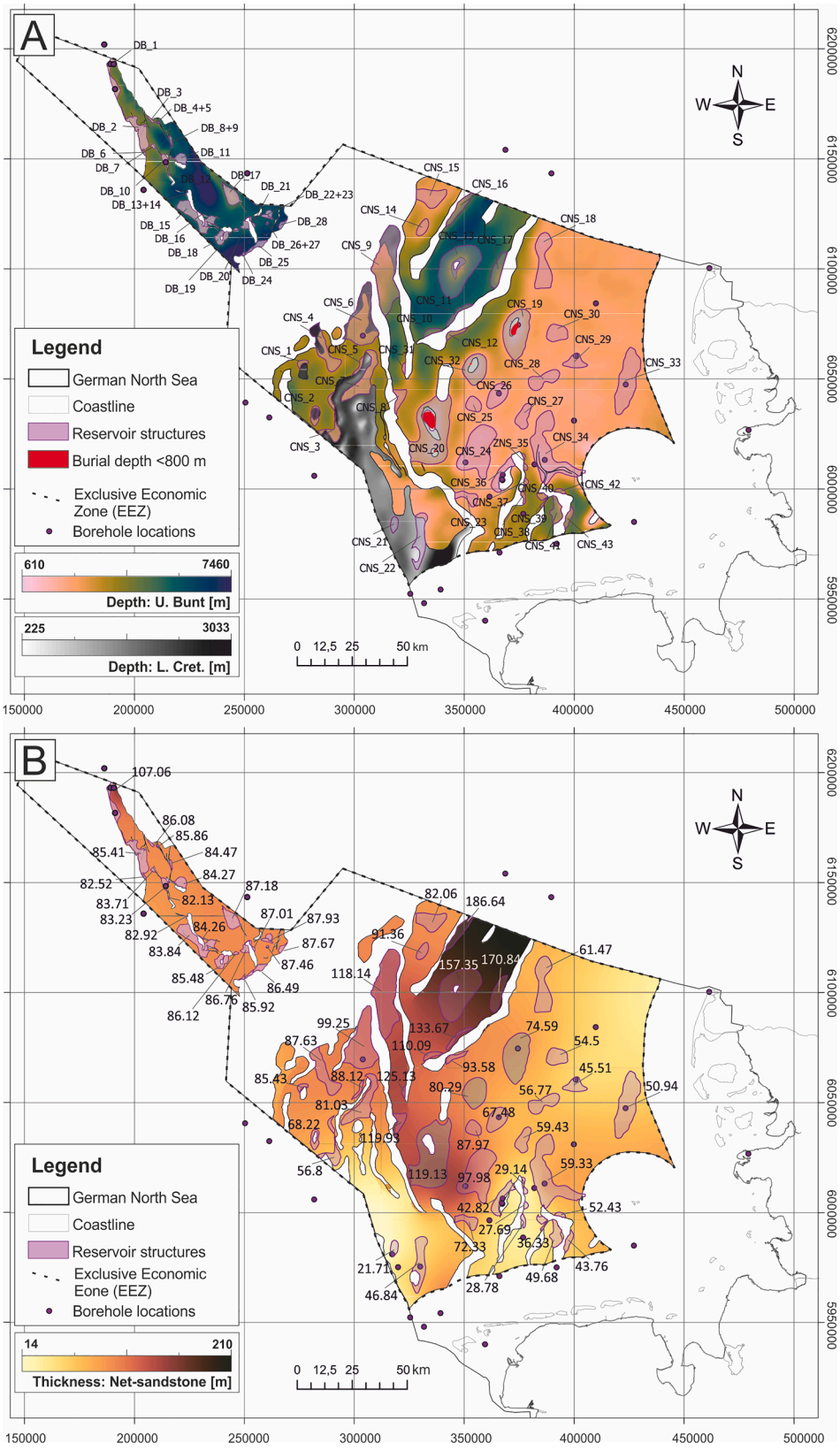

Fig. 3. A) Depth map of the Upper Buntsandstein and Lower Cretaceous (seal formations) and the 71 potential storage sites in the Middle Buntsandstein Subgroup mapped in this study. The Upper Buntsandstein seal is shown in pink to blue colours and the Lower Cretaceous seal in grey scale. Potential storage sites CNS_19, 20 and 32 are excluded from further investigation as their apex depth is above of the threshold of 800 m (grey polygons). B) Net-sandstone thickness distribution of the Middle Buntsandstein Subgroup that were interpreted from well logs and reports of the displayed boreholes. The values refer to the average thickness within the polygon of the potential storage site.

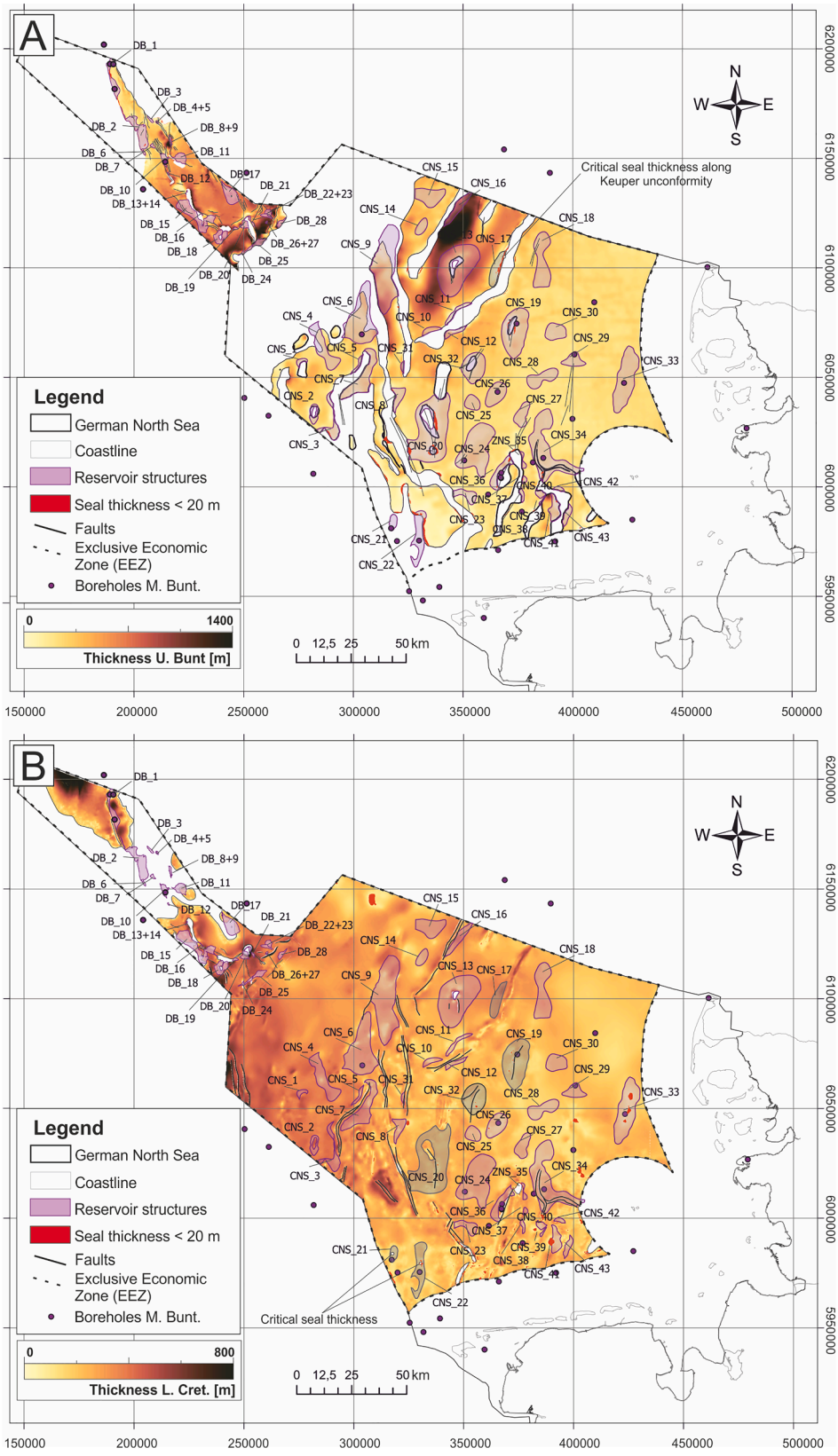

Fig. 4. A) Seal thickness of the Upper Buntsandstein interval. Structure CNS_17 is excluded from further evaluation as the seal thickness is less than 20 m along an unconformity. B) Thickness distribution of the Lower Cretaceous seal unit. Structures CNS_21 and 22 are excluded from further evaluation as the seal thickness is less than 20 m along the L. Cretaceous Unconformity on the G&L Platform.

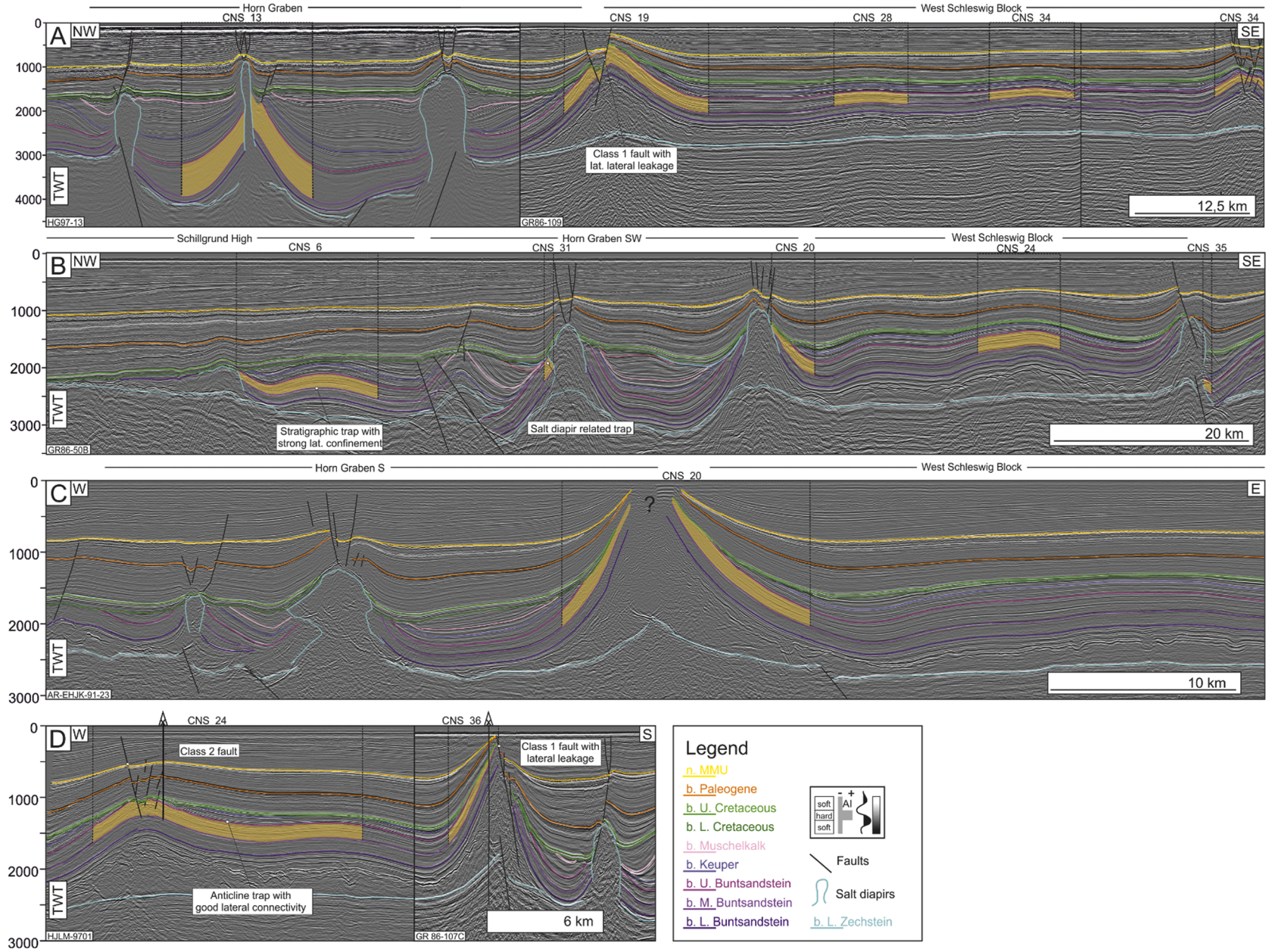

Fig. 5. Seismic cross sections of the central part of the German North Sea. A) Northwest to southeast section across the Horn Graben and the West Schleswig Block. Note the lateral confinement by the salt diapirs associated trap CNS_13 in the Horn Graben. CNS_19 shows a Class 1 fault that reaches the seafloor with lateral leakage potential and an apex depth <800 m. B) Northwest to southeast cross section across the Schillgrund High, the south-western part of the Horn Graben and the West Schleswig Block. Note the stratigraphic trap along the Cretaceous Unconformity and the strong lateral confinement towards the south-western branch of the Horn Graben. C) Seismic cross section across CNS_20, the largest prospect mapped in this study and its missing seal integrity. D) West to southeast cross section showing the laterally unconfined anticline structure of CNS_24 with a Class 2 fault system at its crest (in the south-western part of the structure). CNS_36 is excluded from our further assessment due to a Class 1 fault system and the associated potential for a lateral connection of the reservoir to the shallow overburden. The location of each seismic section is shown in Fig. 1.

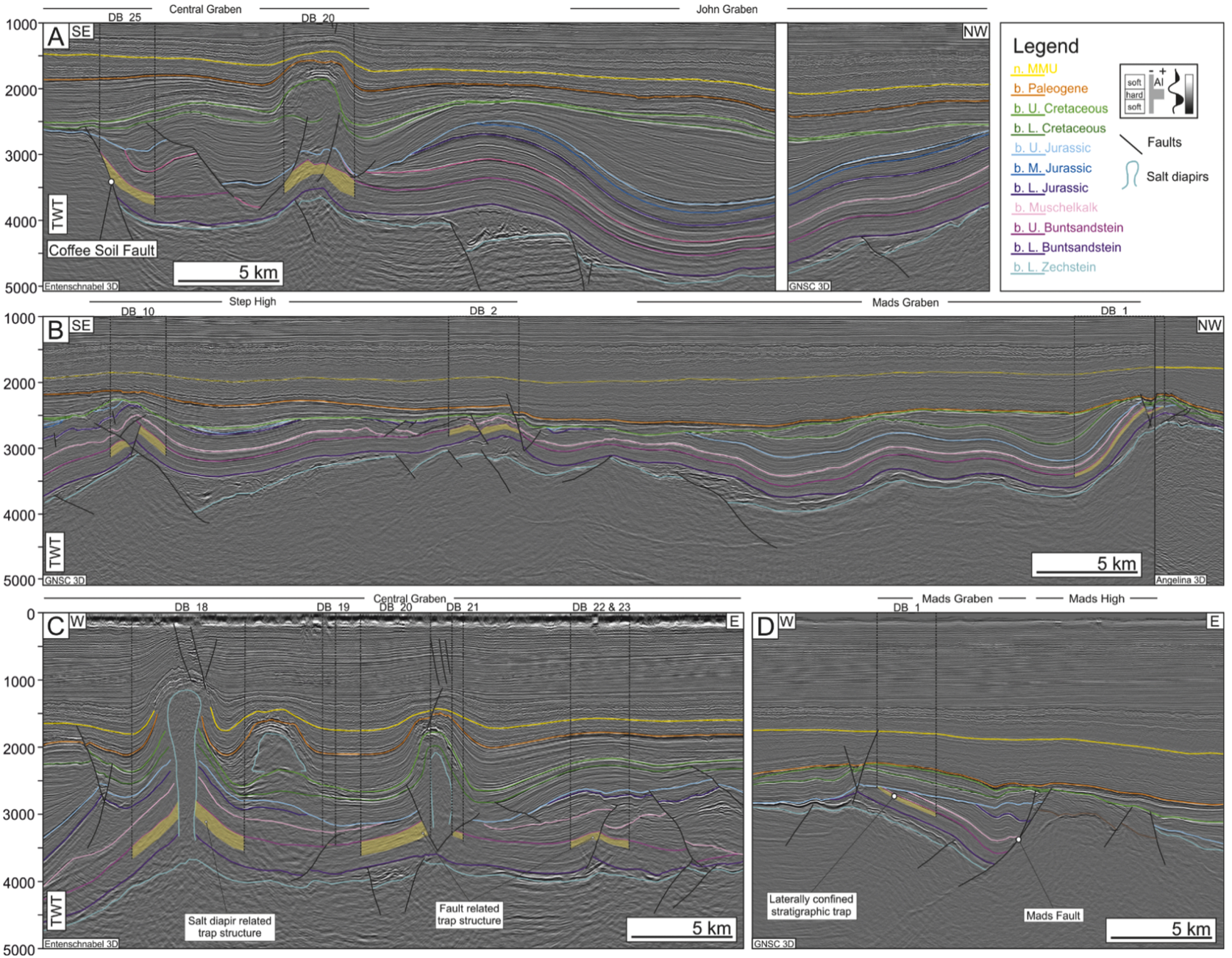

Fig. 6. Seismic section of the Ducks Bill area. A) Southwest – northeast cross section showing the main structural elements of the Central Graben. B) Southwest – northeast cross section showing the distribution main structural elements and potential reservoir structures in the Mads Graben. C) West – east seismic section showing the salt and fault controlled trap structures in the Central Graben area. D) West – east seismic section of the Mads Graben showing the strongly confined stratigraphic trap DB_1. The location of each section is shown in Fig. 1.

Sea area it is very continuous and only locally eroded at the top of some salt pillows and salt diapirs (Fig. 4B). The unconformities along the Schillgund High and G&L Platform are prone to the formation of stratigraphic traps (Fig. 5B). However, seal thickness close to or below the screening threshold of 20 m are recognised along several reservoirs below the Lower Cretaceous Unconformity (CNS_21 & 22) or along local uplifted areas and faults above salt pillows and diapirs (CNS_19, 20 & 32) (Fig. 4B). These trap structures have been excluded for further evaluation in this regional study.

4.2. Traps and storage capacity

The static CO_2 storage capacities are calculated with Monte Carlo simulations (10,000 iterations) to derive a probability distributions of potential CO_2 storage capacities for each trap structure (DR. 4). From these distribution, percentile values of 10 %, 50 % and 90 % are calculated for each structure, in order to represent both conservative and optimistic estimates. The P10 is the value where 10 % of iterations yield lower capacity values, the P50 represents the median and the P90 is the value where 90 % of all iterations yield lower capacity values. The trap structure are genetically linked to the tectonic evolution of the structural domains and are associated with anticlines, faults, salt diapirs, stratigraphic traps or a combination of them. Combined trap styles are in place when one or more sides of a potential storage structure are controlled by a different trapping mechanism than the overall structure. This could be a trap structure that consists of an anticline, with one side closed by a salt diapir.

We mapped a total of 71 traps with an apex depth range between 2400 m to 4962 m in the Ducks Bill and 424 m to 3731 m in the central part of the German North Sea. The deepest trap structures are associated with the Horn, Mads, Step and Central Graben systems. The traps in the Ducks Bill are all located in the Central, Step, and Mads Graben systems and are associated with faults or salt structures or are classified as mixed trap types (Fig. 7A to C). They tend to be relatively small with only 7 out of 28 structures show P50 values above 10 Mt of CO_2 (Fig. 7). Some notable exceptions are the structures DB_2, 15 and 17, which show P50 values between 30 and 50 Mt CO_2. The largest traps (P50 > 50 Mt) are encountered in relatively shallow depths on the West Schleswig Block,

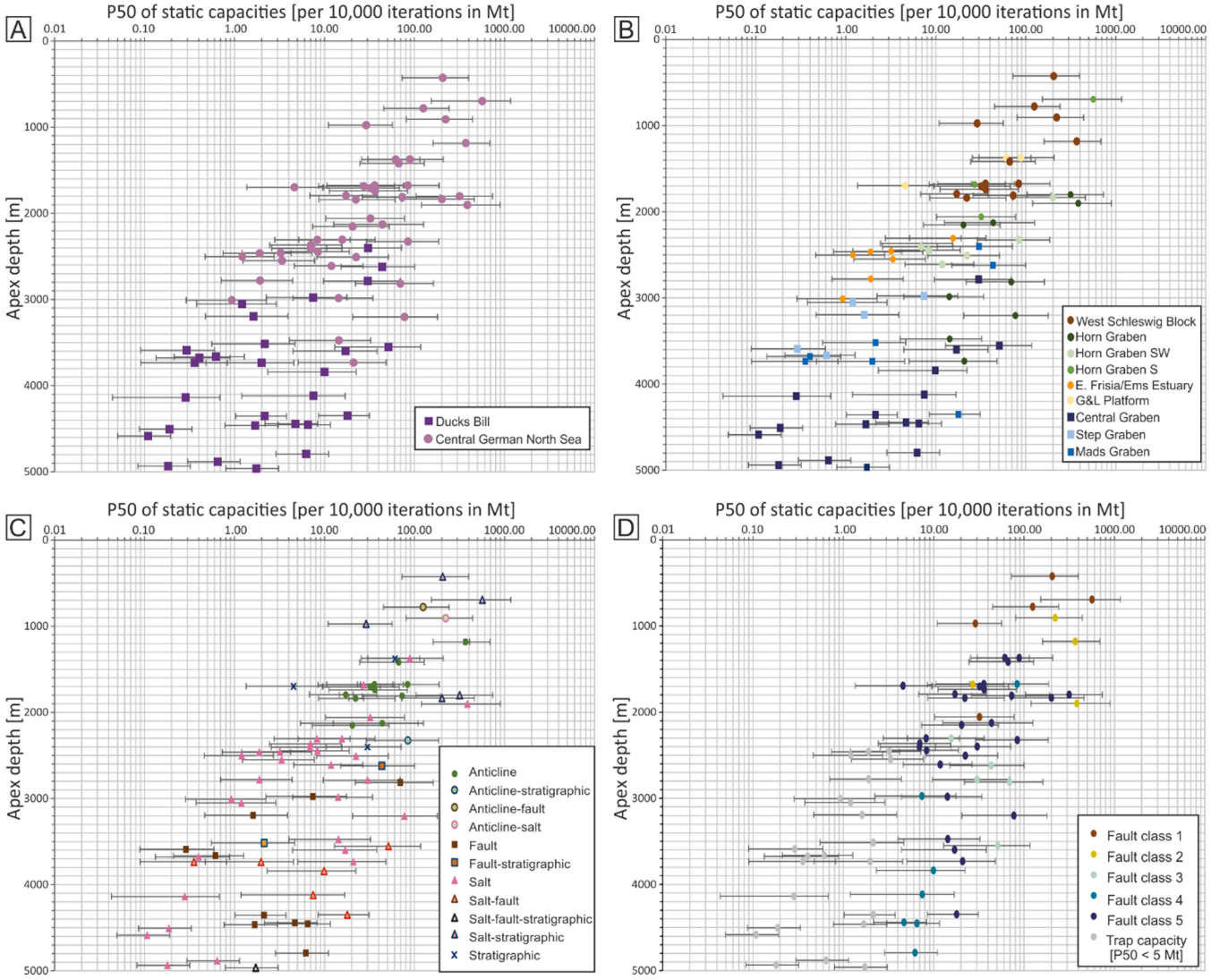

Fig. 7. Average simulated CO_2 storage capacity versus apex depth plots of potential reservoirs in the EEZ of the German North Sea. The range bars show the P10 to P90 likelihood range for each potential CO_2 storage site (DR. 3). A) Potential reservoirs in the Central German North Sea (CNS) and Ducks Bill (DB). B) Potential reservoirs mapped by its structural unit. Note the deep burial and relatively small volumes in the deep graben structures in the Ducks Bill. C) Potential storage sites sorted by trap types. D) Potential storage sites sorted by fault intersections with the main top seal. Note how anticline related traps and their mixed forms are located in the relatively shallow West Schleswig Block and surrounding areas. Whereas the deep-burried and structurally complex graben settings favour the genesis of salt and fault related trap types.

the G&L Platform, and the flanks of the Horn Graben. The eight largest trap structures reaching P50 values > 100 Mt with the largest structure being CNS_20 with a P50 value of 562 Mt CO_2 (Table 1). The West Schleswig Block is dominated by anticline related traps as well as mixed forms combining salt, fault, and stratigraphic traps (Fig. 5, Fig. 7B & C). The East Frisia – Ems Estuary and south-western extension of the Horn Graben are dominated by salt diapir related trap types and show low to medium P50 values (< 1 Mt up to 25 Mt CO_2) with some exceptions (e.g., CNS_4 & CNS_6 in Fig. 3). Anticline related traps and associated mixed trap types show good lateral reservoir connectivity on the West Schleswig Block (Fig. 5). Fault and salt diapir related structures tend to have a high possibility for compartmentalisation due to lateral fluid flow barriers such as salt walls and the juxtaposition of sealing lithologies and reservoir rocks along faults (Fig. 5A, B & Fig. 6C). Stratigraphic traps are relatively rare and associated with erosion during the Early Cretaceous and Upper Jurassic. They occur where Middle Buntsandstein strata is eroded along paleo highs, such as the G&L Platform, the Schillgrund High, or the inverted Mads Graben in the northeast of the German EEZ (Fig. 6D). Similar to structural traps, they tend to have complex geometries and are prone to the occurrence of lateral fluid baffles, especially when they are located close the salt walls (e.g., DB_1 and CNS_6 in Fig. 3A, Fig. 5B & Fig. 6D).

4.3. Structural complexity and fault analysis

To understand potential fluid pathways within storage complexes, their overburden and hydraulically connected units, we analysed the structural complexity around potential reservoir structures in the EEZ of the German North Sea. The intersection lineaments of each fault with the top seal unit of the Upper Buntsandstein, polygonal faults and the seafloor (+100 m) are shown in Fig. 8. Pre-Zechstein faults are commonly in contact with reservoir units along the main structural lineaments of the Mads Fault, the Coffee Soil Fault and the western shoulder of the Horn Graben. They tend to neither have a connection to overlaying non-sealing units, polygonal faults nor reach up to near-seafloor level (Fig. 5 & 6). Salt movement along faults in the pre-Zechstein that reach into Mesozoic strata along the Horn Graben caused a sealing effect and only limited connection between faults and reservoir was mapped in these areas (Fig. 5A). Faults that dominantly displace the Mesozoic are often connected to potential reservoirs of the Middle Buntsandstein Subgroup. They are commonly associated with salt movement on the West Schleswig Block and tectonic activity in the main graben systems. Due to relatively shallow burial depth of potential reservoir rocks on the West Schleswig Block (around 2000 m) they often extend into the Cenozoic strata and in some cases reach the seafloor (Fig. 3A, 5, 7 & 8A). The deeper buried Ducks Bill tends to prevent this extension into young strata, but a connection to the well-developed polygonal fault network can be observed in DB_2, 16 and 17 (Fig. 8B). Based on these cross-cutting relationships, we classified the individual trap structures in five different potential fluid migration systems (Fig. 7D & 8B). We identified five Class 1 structures, where faults from the top of the reservoir reach close to the seafloor with large displacement and potential connectivity into non-sealing units (Fig. 5A, D & 8B). Another four structures show faults from top-reservoir to the seafloor with minor displacement (Class 2) (Fig. 8B). Six of these structures are located on the West Schleswig Block and three in the Horn Graben and its southern extension (CNS_13, 8 und 20). The mapped Class 2 structures show generally large capacities and include six of the largest trap structures (P50 >100 Mt CO_2) (Fig. 5D, 8C & Table 1). Five Class 3 structures with faults in the seal with a potential connection to the polygonal fault system network are mapped in the Central, Mads, Horn Graben and the East Frisia – Ems Estuary areas. Local minor faults (Class 4) in the sealing unit were observed seven times in different locations of the study area. The rest of the potential storage sites show no faults in the top seal of potential reservoirs (Class 5) (Fig. 8B). In addition to fault-reservoir connectivity, the distribution of faults and salt diapirs are important as they can represent lateral fluid barriers and baffles. Mesozoic faults and its associated diapirs are the dominant trap type in the Central Graben (Fig. 7C & 8A). The close proximity and juxtaposition with non-reservoir rocks causes a compartmentalisation, for example structure DB_1 in the Mads Graben (Fig. 6D). The increased fault density in some areas further decrease the size of individual trap structures in the Central and Mads Graben (Fig. 7C). In the central part of the German North Sea diapirism is well-developed along the bounding faults of the Horn Graben and its southern and south-western extension as well as the East Frisia - Ems Estuary region (Fig. 5A-C & 8A). Potential reservoir rocks of the Middle Buntsandstein Subgroup within these structural domains are laterally disconnected and confined. The best lateral connectivity of the Middle Buntsandstein Subgroup is observed on the West Schleswig Block (Fig. 8A). This structural domain is dominated by salt pillows that created latterly open anticline traps or mixed traps associated with them (Fig. 5& 7B-C). Faults tend to be limited to salt pillow and diapir tops and do not pose a major factor for compartmentalisation (Fig. 5).

5. Discussion

5.1. Static CO_2 storage capacities and uncertainties

We calculated the probability distribution of static CO_2 storage capacities via Monte Carlo simulations for 71 individual trap structures in the EEZ of the German North Sea. All parameters included in the calculation (Eq. (1) are associated with individual uncertainties due to limited data availability, data resolution, or geological setting (e.g., structural complexity or salt structures). The accuracy of mapped trap structures, reservoir and seal thickness depend on the resolution of the geological model (regional vs. reservoir scale) as well as the availability and quality of seismic and well data, which strongly vary in the German sector of the North Sea. The Ducks Bill is well covered by 3D seismic data whereas the Central German North Sea dominantly contains 2D seismic lines of different quality and limited spatial coverage (Fig. 1). Additional uncertainties in regional 3D models occur due to velocity anomalies and uncertain mapping of horizons along steeply dipping strata, salt walls, or in deep buried graben structures (Faleide et al., 2021; Hoetz et al., 2011; Jones and Davison, 2014; Wellmann et al., 2010). To account for these uncertainties in the areal extent of individual reservoirs, we added an extra of 5 % standard deviation for each reservoir.

Equally important for the calculation of the overall CO_2 storage capacities, is the net-sandstone thickness. The main targets in the Middle Buntsandstein Subgroup in the EEZ of the German North Sea are the regional continuous basal sandstones of the Volpriehausen, Dethfurth, and Solling Formations (Fig. 2) (Bachmann et al., 2010; Kortekaas et al., 2018). Above each basal sandstones the deposits fine into interbedded silt- and mudstones. A limited long-term sealing potential of these interbedded layers for CO_2 is anticipated, because of analogies with hydrocarbon traps in the Netherlands (Korevaar et al., 2023). Experience of CO_2 storage in the Utsira Sand showed how eight intra-formation mudstones of metre-scale affected the expansion of the CO_2 plume until it reached the main top seal (Cavanagh and Haszeldine, 2014; Chadwick et al., 2004; Hermanrud et al., 2009). We therefore consider the interbedded silt- and mudstones as horizontal fluid flow baffles and barriers that postpone CO_2 migration towards the main top seal of Upper Buntsandstein mudstones and evaporites, and the marine mudstones of the Lower Cretaceous. Due to this migration potential towards the main top seal and good lateral connectivity, all sandstones with a thickness > 1 m within the Middle Buntsandstein Subgroup were included in the net-sandstone thickness estimation. This approach facilitates a good regional overview of the distribution of potential sandstone reservoirs, but cannot reflect local variability in terms of thickness and lateral connectivity. Furthermore, facies variability or diagenetic alterations are not taken into account that affect porosity and permeability distributions (Olivarius et al., 2015). To honour this, an additional standard deviation of 5 % was added to the thickness variability across individual

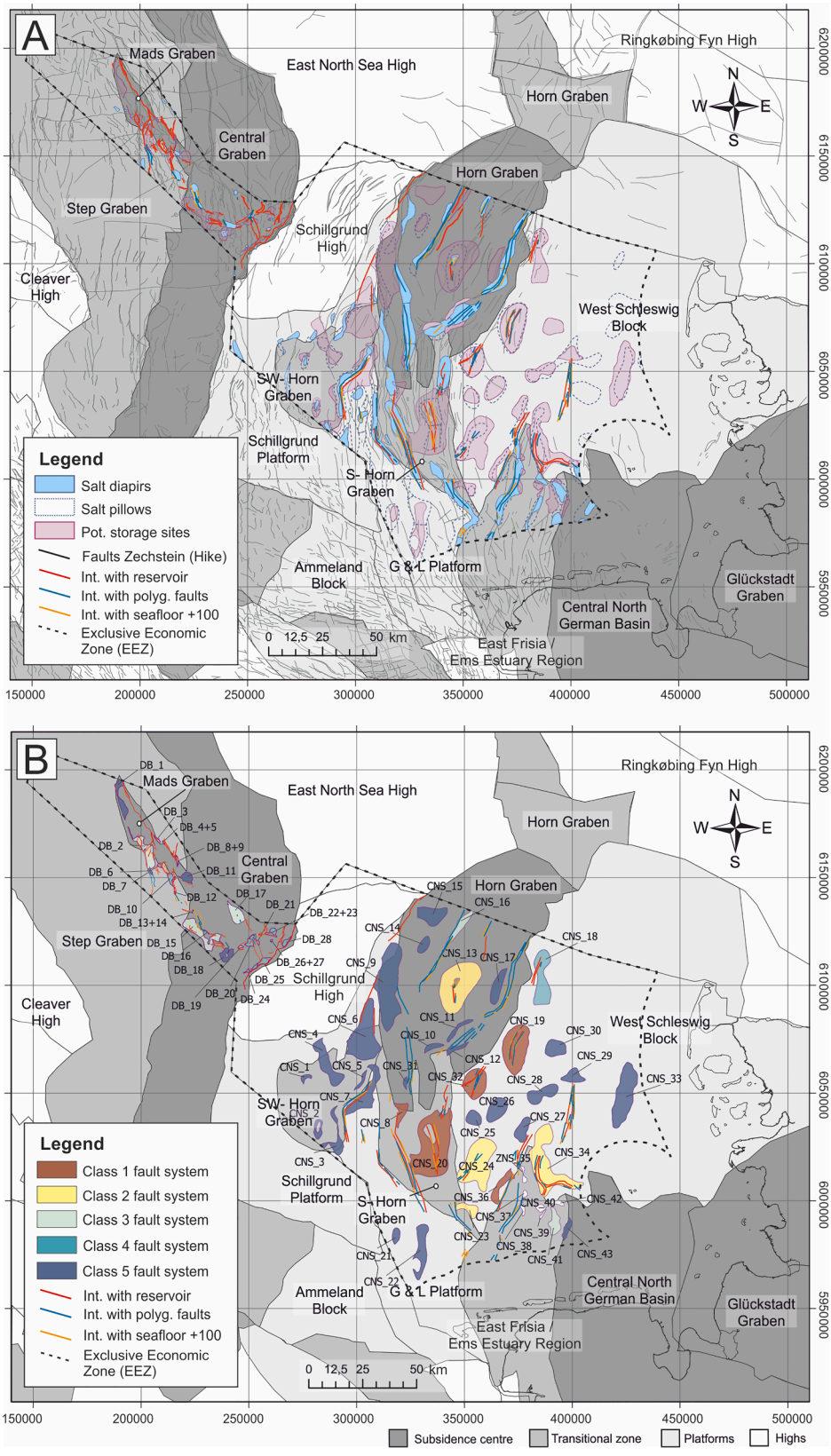

Fig. 8. A) Faults and structures in proximity of the mapped potential reservoir structures in the Middle Buntsandstein Subgroup (Thöle et al., 2022; v. Gessel et al., 2021). Note structural complexity along the main graben systems. B) Fault intersection with the main top seal of each potential reservoir structure based on TUNB faults (Thöle et al., 2022). Class 1 - Faults from the top of the reservoir reaching near the seafloor with large displacement and potential lateral connection to non-sealing units; Class 2 - Faults from the top of the reservoir to the seafloor with minor displacement; Class 3 – Faults in the seal with potential connection to the polygonal fault system; Class 4 - Minor faults in the seal; Class 5 - No faults. Structural elements after Thöle et al. (2021).

trap structures. The limited in-situ porosity data for the Middle Buntsandstein in the German North Sea was offset with available data from the Netherlands (Kortekaas et al., 2018). Although the data are spread across a wide area, the data density (>15,000 data points) enabled us to extract a value range for the depth interval of each reservoir. The resulting likelihood distribution used for the Monte Carlo simulations further buffers the uncertainty in regards of facies distribution within the Buntsandstein interval.

In addition to the data uncertainties, only a certain fraction of the pore space within the trap can be filled by CO_2 as it has to replace in-situ brines during injection (Bachu et al., 2007). The actual amount depends on the complex interaction of different mechanisms such as the dissolution of CO_2 in saline fluids, residual trapping, pressure increase during injection, or well planning and design (Chadwick et al., 2008). The percentage of available pore space that can be effectively filled with CO_2 can be described by an efficiency factor that was established based on numerical simulation and case studies (Haeri et al., 2022; Kopp et al., 2009a, b). We used storage efficiency factors of 5 % to 20 % with a uniformly distribution in the Monte Carlo simulations. This ensures a reasonable certainty range being also in accordance with efficiency ranges used for past capacity assessments (*sensu* Vangkilde-Pedersen et al., 2009; Knopf and May, 2017). Although an efficiency parameter is included, some storage projects show less CO_2 storage capacity during the active sequestration phase of the project (Anthonsen et al., 2016). This effect is buffered by our given likelihood distribution for each reservoir. Dynamic modelling of CO_2 injection on the basis of detailed geological models of individual reservoirs is necessary to verify and refine the estimates of static CO_2 storage capacities presented here.

5.2. Structural complexity, compartmentalisation and potential fluid migration pathways

Depending on the regional stress field, local pressure increases due to CO_2 injection might reactivate existing faults, increase their permeability or induce micro-seismicity (Guglielmi et al., 2021; Rutqvist, 2012). Potential alteration of fault permeability complicates our understanding of regional sealing mechanisms and increases the need for dynamical modelling to better understand fault behaviour (Cappa et al., 2022). Therefore, initial assessments for industrial-scale CO_2 storage needs to take into account fault distribution and orientation to

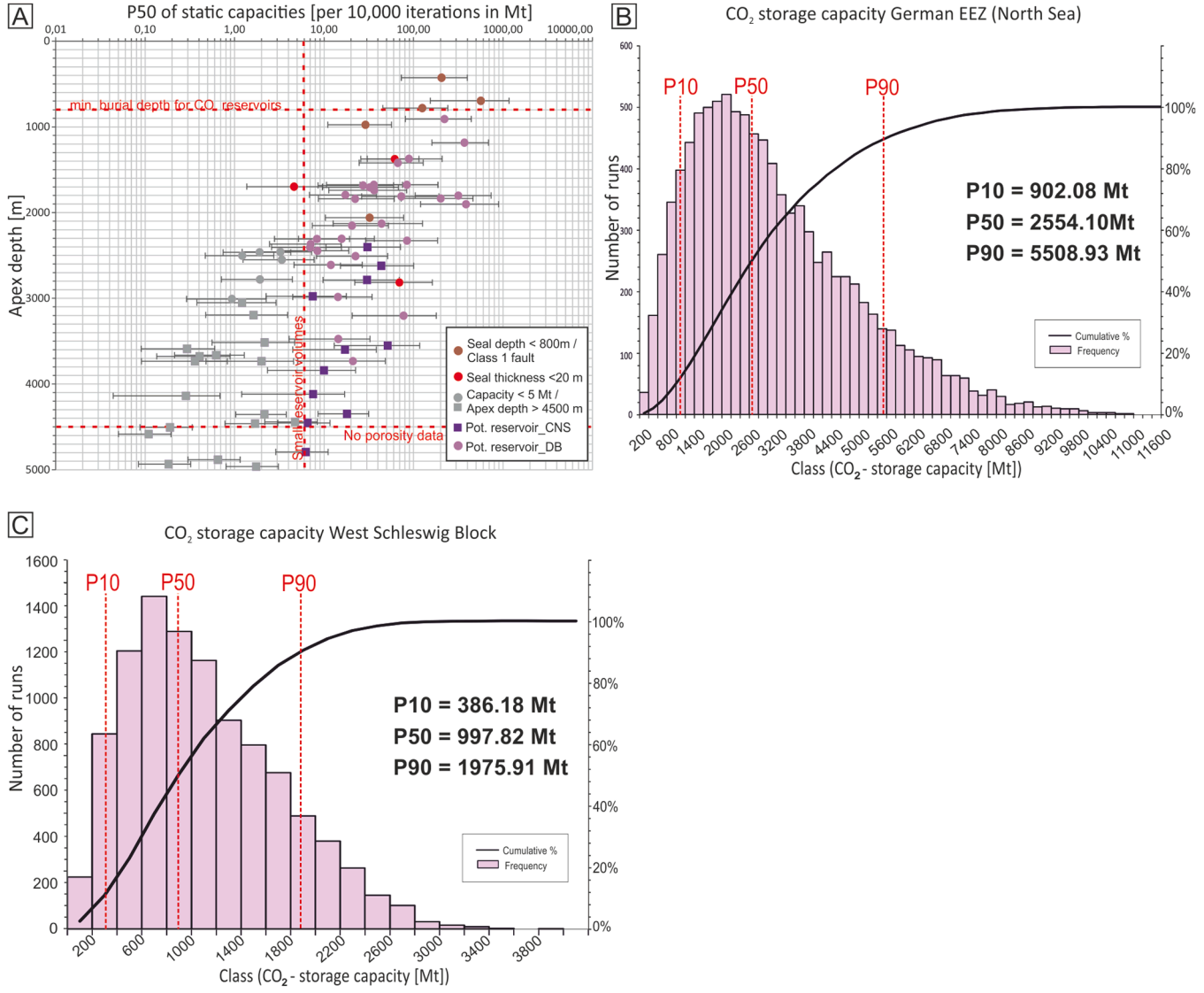

Fig. 9. A) Average simulated CO_2 storage capacity versus apex depth plots of potential reservoirs in the EEZ of the German North Sea. The wings show the P10 and P90 likelihood range for each potential reservoir structure (DR. 3 & 4). B) Probability distribution of all potentially technical feasible reservoir structures that have been positively assessed in the EEZ of the German North Sea. C) Probability distribution of all positively assessed reservoir structures in the West Schleswig Block area, probably representing the promising storage location for CO_2 in the Middle Buntsandstein Subgroup in the German North Sea.

incorporate the necessary resources for further data acquisition towards fault parameterisation and dynamic modelling of fault behaviour and pressure limitation (White and Foxall, 2014). Our mapping shows that seals of several potential storage sites are intersected by faults. Especially, Class 1 faults should be of concern as they reach near the seafloor, show major displacements, and have a potential to act as fluid migration pathways into adjacent non-sealing units. Reservoirs associated with such faults should be excluded in the exploration ranking, especially if they are shallow and have a reservoir apex depth less than 800 m, such as CNS_19, 20 and 32 (Fig. 5A-C, 7D & 9A). Reservoirs that are intersected by Class 2 faults are often associated with salt pillow growth or diapirism causing crestal faulting of the top seal that reaches close to the seafloor (Fig. 5D & 8C). The four structures (CNS_13, 23, 24 and 34) associated with these faults are included in the overall capacity calculation, but demand careful evaluation and modelling to determine their suitability for storing supercritical CO_2. Structures CNS_24 and 34 are of greatest interest, as they can potentially store large capacities of CO_2 and are in an open to semi-open system on the West Schleswig Block (Fig. 5D, 9 & 10). This hydraulic connectivity may facilitate good pressure dissemination along the laterally well-connected sandstone beds, and injection pressures could stay below the faults reactivation pressures. CNS_13 is, although the second largest structure, less favourable due to its location in the Horn Graben (Fig. 5A & 9). Potentially high initial pressures, uncertainty of reservoir quality and the confined setting of the Horn Graben increase the chance for relatively low storage efficiency and fault reactivation (Rutqvist, 2012; Tillner et al., 2013; Zhou et al., 2008). Polygonal fault networks, especially those connected to top seal faults, require thorough investigation to assess their potential as fluid pathways (Class 3). Trap structures with a potential connection to polygonal fault networks are mainly located in the Ducks Bill with DB_2, DB and 17 being the largest structures in the area (Fig. 6, 9 & 10). There are bright spots associated with shallow gas accumulations mapped above DB_15, which could indicate fluid migration pathways along faults (Müller et al., 2018). The origin of these gas accumulations is not fully known. One possibility is the upwards migration of gas from Jurassic source rocks (Müller et al., 2020), or as suggested by studies in the Netherlands a microbial origin (de Bruin et al., 2022). Although bright spots and chimneys are a good indicator for fluid migration, there need to be fluids in place to recognize prior to CO_2 injections. Also, vertical acoustic blanking may be associated with fluid migration structures have been shown to be caused by gas accumulations in paleo fluvial channels or paleo valleys (Ahlrichs et al., 2024; de Bruin et al., 2022). Regardless of fluid indicators in place, polygonal faults are associated with fluid migration in other geological systems and a thorough investigation of fault reactivation and seal integrity needs to be carried out for these potential storage sites (Hustoft et al., 2007). Storage sites devoid of significant faults in the seal are considered the most promising sites for further exploration (Class 4 and 5).

Additionally to potential fluid migration pathways, the structural complexity of a CO_2 storage site plays a crucial role in its performance and safety. Lateral barriers that limit fluid movement can prevent pressure equilibration between subsurface volumes, when CO_2 displaces in-situ brines, thus increasing reservoir pressures (Birkholzer et al., 2015). This pressure increase in closed or semi-closed aquifers limits the CO_2 storage capacity of individual reservoirs and others nearby (Birkholzer and Zhou, 2009; Schäfer et al., 2012; Zhou and Birkholzer, 2011). Strong compartmentalisation can be observed in possible storage

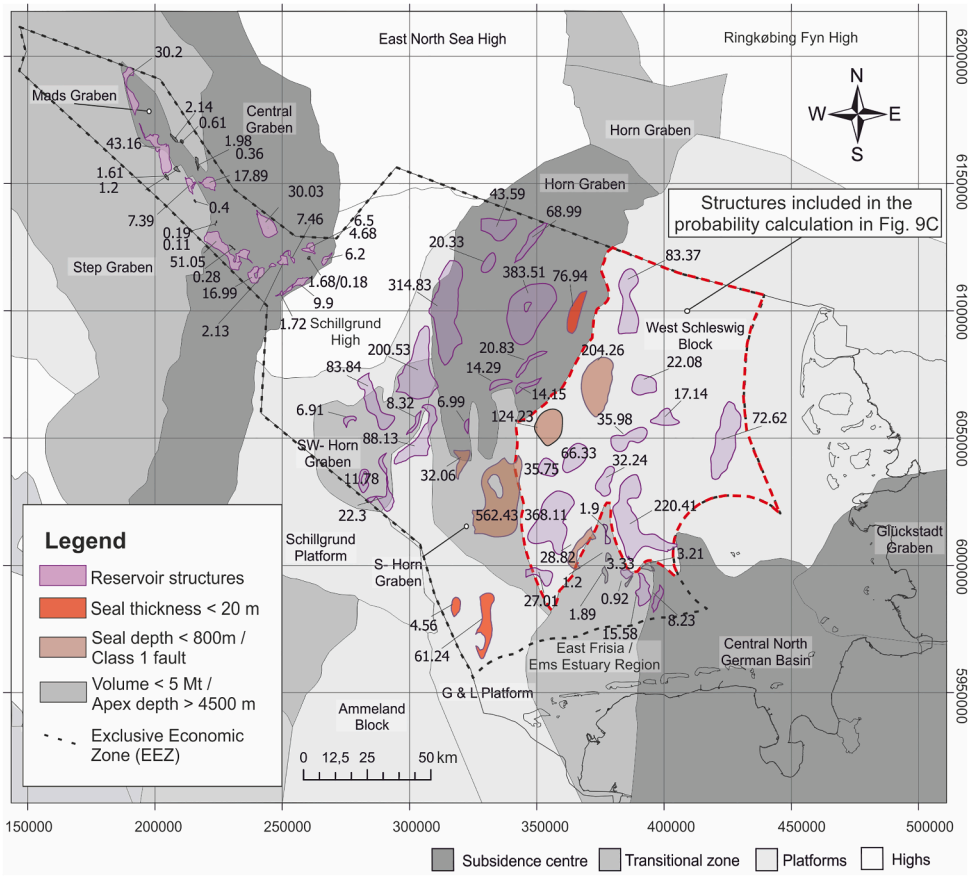

Fig. 10. Potential reservoir structures for CO_2 storage in the EEZ of the German North Sea in the Middle Buntsandstein Subgroup including the main structural domains. The red outline marks the West Schleswig Block, which shows the best overall conditions for the sequestration of CO_2 in the Buntsandstein Subgroup in the German North Sea. Structural domains after Thöle et al. (2021).

sites located in the Mads, Central, and Horn Graben, where faults and salt diapirs could restrict lateral fluid flow (Fig. 4, 5 & 6). The limiting effect of high pressure on CO_2 storage capacity is enhanced if the Middle Buntsandstein reservoirs in the deep parts of the graben structures underwent inversion and are subject to natural overpressures (Peeters et al., 2018). These sites may be less advantageous than others as they are prone to increased drilling risks and static storage capacities may be overestimated compared to dynamic capacity assessments. If not over-pressured, deep-buried reservoir structures can be prone to diagenetic cementation effects that facilitate the deterioration of reservoir quality (Bjørlykke, 2014). Similarly complex and prone to overpressure generation are the stratigraphic traps and mixed trap types associated with these, such as DB_1 in the Mads Graben and CNS_9 and 6 along the Schillgrund High (Fig. 5B & 8). These reservoir structures consist of dipping beds with a hydraulic connection with the deeper parts of the basin, a lateral flow barrier due to faults (DB_1) or salt walls (CNS_9), and a sealing unit above an erosive unconformity at the top of the structure (Fig. 5B & 6D). The evaluation of faults and salt diapirs in terms of potential fluid migration and reservoir compartmentalisation showed that the West Schleswig Block is the most suitable area in the EEZ of the German North Sea for further exploration and the selection of a suitable CO_2 storage site.

5.3. Potential storage site evaluation

We give a complete overview of the existing potential CO_2 storage sites and their static storage capacity in the EEZ of the German North Sea (Fig. 10, DR. 2 & 4). Some of these mapped storage sites appear more suitable for further investigation in terms of storage capacity, trap type, hydraulic connectivity, burial depth and potential fluid migration pathways. We apply cut off criteria to distinguish less suitable reservoirs from more promising ones. We further rank and discuss the most favourable reservoir structures that should be selected for further in depth dynamic modelling of multiphase flow systems to calculate rigid CO_2 storage capacities. The cut off criteria are a minimum burial depth of >800 m, a seal thickness of 20 m, a minimum P50 of >5 Mt CO_2, and a maximum apex depth of 4500 m (Fig. 9A). The maximum depth is related to likely economically and geotechnically reasonable drilling depth, pressure distribution, and limited availability of porosity data in depths greater than 4500 m (Kortekaas et al., 2018).

A total of 24 potential storage sites can be excluded due to their capacity and burial depth (Fig.9A). Most of them are located in the deeply buried Mads, Central and Step Graben systems, where there is the additional high chance for lateral compartmentalisation. Another three reservoirs are excluded based on thin top seals (CNS_17, 21 and 22) (Fig.4A & B). Further five reservoirs are excluded due to their low apex depth (< 800 m), occurrence of Class 1 faults in their top seal and a potential of lateral fluid migration into non-sealing units (CNS_8, 19, 20, 32 and 36) (Fig. 10). A Monte Carlo simulation with the remaining potential reservoir structures gives a likelihood distribution of static storage capacities with associated percentiles at P10 = 902.08 Mt, P50 = 2554.10 Mt, and P90 = 5508.93 Mt (Fig. 9B). However, it is not certain that the whole capacities are available due to the discussed uncertainties, such as compartmentalisation or regional pressure build-up in storage formations caused by the interference of storage sites (Birkholzer et al., 2015; Schäfer et al., 2012).

Our 20 best ranking prospects with respect to the median (P50) of potential storage capacity are highlighted in Table 1. The largest structures are generally located in the Central German North Sea with two exceptions in the Central and Mads Graben (DB_15 and 2) (Fig. 10). Three of these top 20 structures are excluded from the overall capacity estimates as their apex depth is below the defined 800 m threshold and their top seal is cut by Class 1 faults (CNS_20, 19 and 32) (Fig. 8B & 10). One more trap is excluded as the local seal thickness is < 20 m (CNS_22). Further three structures with considerable capacities have top seals with Class 2 faults (CNS_13, 24 and 34). This may be a limiting factor in terms of injection pressure and the need for increased resources for geotechnical modelling, site characterization and monitoring (Ward et al., 2016). Especially structures CNS_24 and 34 are interesting options for further exploration due their potentially high capacity and good lateral reservoir connectivity on the West Schleswig Block. These unconfined anticline trap structures allow for a spatial pressure distribution and dissipation, being more favourable over confined ones. Structure CNS_9, for example, has a large anticipated storage capacity with a P50 value of 314 Mt CO_2, but the stratigraphic trap type in combination with the lateral confinement along salt walls make it less favourable compared to unconfined structures. The dynamic storage capacity may be less than predicted as high natural fluid pressures may occur along the dipping high permeable strata that would be further increased by CO_2 injection (Birkholzer et al., 2015; Peeters et al., 2018).

A regional storage in adjacent structures may be an option to develop injection strategies for several of the individual reservoirs discussed in this study and the utilisation of pore volumes between them. The geologically most suitable area would be the well-connected reservoir sandstones on the West Schleswig Block with open anticline traps and little to no lateral confinement. The investigated trap structures on the West Schleswig Block alone show static CO_2 storage capacity probabilities of P10 = 386.18 Mt, P50 = 997.82 Mt, and P90 = 1975.91 Mt (Fig. 9C). When the space in between these structure is included, capacities could increase further. This approach would need additional work to model injection schemes and the regional migration of CO_2 streams and formation water to utilize individual traps in a fill and spill approach (Nilsen et al., 2015; Patruno et al., 2024). It would be crucial to exclude structures CNS_20, 19 and 32 due to their Class 1 faults in the top seal and the shallow apex depth of these structures. Although detailed exploration of such a large area would need considerable resources, a coordinated regional injection strategy could be developed. Thus, provided sites and strategy are found to be suitable, the exploitation of the available CO_2 storage capacity in the German North Sea could be optimized. It has to be stressed that the work presented in this article is based on geological considerations only. The success of CO_2 projects will depend on other factors as well, such as environmental, economical, legal or spatial planning constraints.

6. Future work

The precise storage potential of a trap within a saline aquifer depends on a variety of factors such as the pore volume, the permeability, the achievable CO_2 saturation, the dissolution of CO_2 in saline pore fluids, residual trapping potential and pressure distribution that may limit CO_2 injection (Chadwick et al., 2008). Future work on the dynamic reservoir and geotechnical modelling of individual potential storage sites is needed to verify the outlined storage potential and safety considerations (Bachu, 2015). An effective research strategy could involve selecting two structures with variable settings, e.g., covering an anticline structure characterized by strong lateral aquifer connectivity and a more intricate reservoir type within a confined setting. Potential candidates would be CNS_24 and DB_1 as they would provide endmembers for anticline and stratigraphic traps in laterally open and strongly confined aquifer systems (Fig. 3 & 5D). Both of these reservoirs are directly targeted by exploration wells to provide the necessary data for further modelling efforts. For fault associated trap types geotechnical modelling should focus on the fault reactivation and leakage potential to constrain safe injection pressure ranges and monitoring strategies (Ward et al., 2016; Wu et al., 2021). For detailed investigations in the West Schleswig Block additional 3D seismic and well data would be necessary to lower the uncertainty in terms of reservoir geometry, fault distribution, and parametrisation. Additional efforts could focus on the evaluation of legacy well data and regional parametrisation of promising areas, such as the West Schleswig Block, to aid the development of large scale CCS in the German North Sea. To facilitate further data acquisition and the development of large scale CCS projects in the German North Sea a joint

effort of research, industry and political stakeholders is crucial.

7. Conclusion

We undertook a comprehensive analysis of potential CO_2 storage sites in the Middle Buntsandstein Subgroup within the Exclusive Economic Zone of the German North Sea. We mapped 71 potential storage sites based on existing 3D models, seismic data and a total of 39 existing exploration wells. Employing Monte Carlo simulations with 10,000 iterations, we created probability functions for likely static CO_2 storage volumes for each of the mapped structures. Each of these structures underwent further characterisation based on static storage capacity, burial depth, trap type and structural complexity. Structures with a P50 $<$ 5 Mt and those deeply buried below 4500 m were excluded from the total capacity balance, due to geotechnical feasibility concerns. Additionally, structures with apex depths of less than 800 m, cumulative seal thickness $<$ 20 m, and potential fluid migration pathways along major faults were excluded. The remaining structures yield a probability distribution of static CO_2 storage capacities (of all suitable structures) at P10 = 902.08 Mt, P50 = 2554.10 Mt, and P90 = 5508.93 Mt. Structures in deeply buried graben structures or complex fault and salt diapir-related trap structures are prone to lateral confinement, which presents challenges in terms of pressure increase during injection and capacity prediction. Conversely, favourable conditions are expected on the West Schleswig Block, including moderate burial depths, anticline dominated trap types and good lateral reservoir connectivity. Geologically the West Schleswig Block stands out as the most promising target for further exploration of carbon storage sites in the EEZ of the German North Sea, offering a probability distribution of static CO_2 storage capacities of all suitable structures yielding percentiles at P10 = 386.18 Mt, P50 = 997.82 Mt, and P90 = 1975.91 Mt. We emphasize the necessity for additional data acquisition and recommend further dynamic modelling of CO_2 storage for individual trap structures. Both will be needed for the realisation of safe and effective storage projects in the in the deep subsurface of the German North Sea.

CRediT authorship contribution statement

A. Fuhrmann: Writing – review & editing, Writing – original draft, Investigation, Conceptualization, Methodology, Visualization. **S. Knopf:** Writing – review & editing, Writing – original draft, Methodology, Formal analysis, Conceptualization. **H. Thöle:** Writing – review & editing, Software, Investigation, Data curation. **F. Kästner:** Writing – review & editing, Methodology, Formal analysis, Software. **N. Ahlrichs:** Writing – review & editing, Investigation. **H.L. Stück:** Writing – review & editing, Investigation. **A. Schlieder-Kowitz:** Writing – review & editing, Investigation. **G. Kuhlmann:** Writing – review & editing, Project administration, Funding acquisition.

Declaration of competing interest

The authors declare that they have no known competing financial interests or personal relationships that could have appeared to influence the work reported in this paper.

Data availability

All input data is listed in the Supplementary Material (DR. 1 & 2). Seismic and well data are available according to the Geological Data Act (GeolDG).

Acknowledgements

We would like to thank two anonymous reviewers for their constructive comments and help to improve this manuscript. This study was funded by the Federal Ministry of Education and Research of Germany (BMBF) in the framework of GEOSTOR (project number 03F0893B), one of the six research consortia of the German Marine Research Alliance (DAM) research mission “Marine carbon sinks in decarbonisation pathways” (CDRmare). We thank AspenTech for providing Paradigm/EPOS Software Package licenses via the Academic Software Program (https://www.aspentech. com/en/academic-program) to support BGR as a national geological service in non-profit work for the public and education. The authors declare that they have no known competing financial interests or personal relationships that could have appeared to influence the work reported in this paper. Open Access funding enabled and organized by Project DEAL.

Supplementary materials

Supplementary material associated with this article can be found, in the online version, at doi:10.1016/j.ijggc.2024.104175.

References

Ahlrichs, N., Ehrhardt, A., Schnabel, M., Berndt, C., 2024. Vertical acoustic blanking in seismic data from the German North Sea: a spotlight to shallow gas-bearing incised channels. J. Quat. Sci. 39, 421–431. https://doi.org/10.1002/jqs.3590.

Anthonsen, K.L., Bernstone, C., Feldrappe, H., 2014. Screening for CO_2 storage sites in Southeast North Sea and Southwest Baltic Sea. Energy Proc. 63, 5083–5092. https://doi.org/10.1016/j.egypro.2014.11.538.

Anthonsen, K.L., Frykman, P., Møller Nielsen, C., 2016. Mapping of the CO_2 storage potential in the Nordic region. Geol. Surv. Den. Greenl. Bull. 35, 87–90. https://doi.org/10.34194/geusb.v35.4946.

Arfai, J., Jähne, F., Lutz, R., Franke, D., Gaedicke, C., Kley, J., 2014. Late Palaeozoic to early Cenozoic geological evolution of the northwestern German North Sea (Entenschnabel): New results and insights. Neth. J. Geosci. - Geol. Mijnb. 93, 147–174. https://doi.org/10.1017/njg.2014.22.

Bachmann, G.H., Geluk, M.C., Warrington, G., Becker-Roman, A., Beutler, G., Hagdorn, H., Hounslow, M.W., Nitsch, E., Röhling, H.-G., Simon, T., Szulc, A., 2010. Triassic. In: Doornenbal, J.C., Stevenson, A.G. (Eds.), Petroleum Geological Atlas of the Southern Permian Basin Area. EAGE Publications B.V., Houten, pp. 148–173.

Bachmann, G.H., Hoffmann, N., 1997. Development of the Rotliegend basin in Northern Germany. Geol. Jahrb. D 103, 9–31.

Bachu, S., 2015. Review of CO_2 storage efficiency in deep saline aquifers. Int. J. Greenh. Gas Con. 40, 188–202. https://doi.org/10.1016/j.ijggc.2015.01.007.

Bachu, S., Bonijoly, D., Bradshaw, J., Burruss, R., Holloway, S., Christensen, N.P., Mathiassen, O.M., 2007. CO_2 storage capacity estimation: methodology and gaps. Int. J. Greenh. Gas Con. 1, 430–443. https://doi.org/10.1016/s1750-5836(07)00086-2.

Baumgarten, C., Patel, T., 2022. Automatic random variate generation in Python. SciPy 46–51.

Bense, F., Deutschmann, A., Dzieran, L., Hese, F., Höding, T., Jahnke, C., Lademann, K., Liebsch-Dörschner, T., Müller, C.O., Obst, K., Offermann, P., Schilling, M., Wächter, J., 2022. Potenziale des unterirdischen Speicher- und Wirtschaftsraumes im Norddeutschen Becken (TUNB) - Phase 2: Parametrisierung. Abschlussbericht. Bundesanstalt für Geowissenschaften und Rohstoffe (BGR) 193.

Bense, F.A., Jähne-Klingberg, F., 2017. Storage potentials in the deeper subsurface of the central German North Sea. Energy Proc. 114, 4595–4622. https://doi.org/10.1016/j.egypro.2017.03.1580.

Bentham, M., Mallows, T., Lowndes, J., Green, A., 2014. CO_2 storage evaluation database (CO_2 Stored). The UK's online storage atlas. Energy Proc. 63, 5103–5113. https://doi.org/10.1016/j.egypro.2014.11.540.

Birkholzer, J.T., Oldenburg, C.M., Zhou, Q., 2015. CO_2 migration and pressure evolution in deep saline aquifers. Int. J. Greenh. Gas Con. 40, 203–220. https://doi.org/10.1016/j.ijggc.2015.03.022.

Birkholzer, J.T., Zhou, Q., 2009. Basin-scale hydrogeologic impacts of CO_2 storage: capacity and regulatory implications. Int. J. Greenh. Gas Con. 3, 745–756.

Bjørlykke, K., 2014. Relationships between depositional environments, burial history and rock properties. Some principal aspects of diagenetic process in sedimentary basins. Sediment. Geol. 301, 1–14. https://doi.org/10.1016/j.sedgeo.2013.12.002.

Bouroullec, R., Verreussel, R.M.C.H., Geel, C.R., de Bruin, G., Zijp, M.H.A.A., Kőrösi, D., Munsterman, D.K., Janssen, N.M.M., Kerstholt-Boegehold, S.J., 2018. Tectonostratigraphy of a rift basin affected by salt tectonics: synrift middle jurassic–lower cretaceous dutch central graben, terschelling basin and neighbouring platforms, Dutch offshore. Geol. Soc. 469, 269–303. https://doi.org/10.1144/sp469.22. London, Special Publications.

Bourquin, S., Guillocheau, F., Péron, S., 2009. Braided rivers within an arid alluvial plain (example from the Lower Triassic, western German Basin): recognition criteria and expression of stratigraphic cycles. Sedimentology 56, 2235–2264. https://doi.org/10.1111/j.1365-3091.2009.01078.x.

Brown, A.R., 2001. Calibrate yourself to your data! A vital first step in seismic interpretation. Geophys. Prospect. 49, 729–733. https://doi.org/10.1046/j.1365-2478.2001.00284.x.

Buchanan, P.G., Bishop, D.J., Hood, D.N., 1996. Development of salt-related structures in the Central North Sea: results from section balancing. Geol. Soc. 100, 111–128. https://doi.org/10.1144/gsl.Sp.1996.100.01.09. London, Special Publications.

Cappa, F., Guglielmi, Y., De Barros, L., 2022. Transient evolution of permeability and friction in a slowly slipping fault activated by fluid pressurization. Nat. Commun. 13, 3039. https://doi.org/10.1038/s41467-022-30798-3.

Cavanagh, A.J., Haszeldine, R.S., 2014. The Sleipner storage site: capillary flow modeling of a layered CO_2 plume requires fractured shale barriers within the Utsira formation. Int. J. Greenh. Gas Con. 21, 101–112. https://doi.org/10.1016/j.ijggc.2013.11.017.

Celia, M.A., 2017. Geological storage of captured carbon dioxide as a large-scale carbon mitigation option. Water. Resour. Res. 53, 3527–3533. https://doi.org/10.1002/2017wr020841.

Chadwick, A., Arts, R., Bernstone, C., May, F., Thibeau, S., Zweigel, P., 2008. Best practice for the storage of CO2 in saline aquifers-observations and guidelines from the SACS and CO2STORE projects.

Chadwick, R.A., Zweigel, P., Gregersen, U., Kirby, G.A., Holloway, S., Johannessen, P.N., 2004. Geological reservoir characterization of a CO_2 storage site: the Utsira sand, Sleipner, northern North Sea. Energy 29, 1371–1381. https://doi.org/10.1016/j.energy.2004.03.071.

Damen, K., Faaij, A., Turkenburg, W., 2009. Pathways towards large-scale implementation of CO_2 capture and storage: a case study for the Netherlands. Int. J. Greenh. Gas Con. 3, 217–236. https://doi.org/10.1016/j.ijggc.2008.09.005.

de Bruin, G., ten Veen, J., Wilpshaar, M., Versteijlen, N., Geel, K., Verweij, H., Carpentier, S., 2022. Origin of shallow gas in the Dutch North Sea — Seismic versus geochemical evidence. Interpretation 10, SB63–SB76. https://doi.org/10.1190/int-2021-0081.1.

de Jager, J., 2003. Inverted basins in the Netherlands, similarities and differences. Neth. J. Geosci. 82, 339–349. https://doi.org/10.1017/S0016774600020175.

de Jager, J., 2014. The discovery of the fat sand play (solling formation, triassic), northern Dutch offshore – a case of serendipity. Neth. J. Geosci. - Geol. Mijnb. 91, 609–619. https://doi.org/10.1017/s0016774600000408.

Dethlefsen, F., Ebert, M., Dahmke, A., 2014. A geological database for parameterization in numerical modeling of subsurface storage in northern Germany. Environ. Earth Sci. 71, 2227–2244. https://doi.org/10.1007/s12665-013-2627-1.

Dèzes, P., Schmid, S.M., Ziegler, P.A., 2004. Evolution of the European Cenozoic rift system: interaction of the Alpine and Pyrenean orogens with their foreland lithosphere. Tectonophysics 389, 1–33. https://doi.org/10.1016/j.tecto.2004.06.011.

Doornenbal, H., Dulk, M.d., Thöle, H., Jähne-Klingberg, F., Breitzke, P., Jakobsen, F., 2021. Deliverable 3.7 A harmonized cross-border velocity model, GEOERA 3D GEO-EU 3D geomodeling for Europe project number: GeoE.171.005.

Faleide, T.S., Braathen, A., Lecomte, I., Mulrooney, M.J., Midtkandal, I., Bugge, A.J., Planke, S., 2021. Impacts of seismic resolution on fault interpretation: insights from seismic modelling. Tectonophysics 816. https://doi.org/10.1016/j.tecto.2021.229008.

Fontaine, J.M., Guastella, G., Jouault, P., de la Vega, P., 1993. F15-A: a triassic gas field on the eastern limit of the Dutch Central Graben. Geol. Soc. 4, 583–593. https://doi.org/10.1144/0040583. London, Petroleum Geology Conference Series.

Geluk, M., McKie, T., Kilhams, B., 2018. An introduction to the Triassic: current insights into the regional setting and energy resource potential of NW Europe. Geol. Soc. 469, 139–147. https://doi.org/10.1144/sp469.1. London, Special Publications.

Geluk, M.C., 2005. Stratigraphy and tectonics of Permo-Triassic basins in the Netherlands and surrounding areas. PhD Thesis. Utrecht University.

Geluk, M.C., Röhling, H.G., 1997. High-resolution sequence stratigraphy of the lower Triassic 'Buntsandstein' in the Netherlands and northwestern Germany. Geol. Mijnb. (Geol. Min.) 76, 227–246. https://doi.org/10.1023/a:1003062521373.

Guglielmi, Y., Nussbaum, C., Cappa, F., De Barros, L., Rutqvist, J., Birkholzer, J., 2021. Field-scale fault reactivation experiments by fluid injection highlight aseismic leakage in caprock analogs: implications for CO_2 sequestration. Int. J. Greenh. Gas Con. 111 https://doi.org/10.1016/j.ijggc.2021.103471.

Haeri, F., Myshakin, E.M., Sanguinito, S., Moore, J., Crandall, D., Gorecki, C.D., Goodman, A.L., 2022. Simulated CO_2 storage efficiency factors for saline formations of various lithologies and depositional environments using new experimental relative permeability data. Int. J. Greenh. Gas Con. 119 https://doi.org/10.1016/j.ijggc.2022.103720.

Halland, E.K., Riis, F., Magnus, C., Johansen, W.T., Tappel, I.M., Gjeldvik, I.T., Solbakk, T., Pham, V.T.H., 2013. CO_2 storage atlas of the Norwegian part of the North Sea. Energy Proc. 37, 4919–4926. https://doi.org/10.1016/j.egypro.2013.06.403.

Hermanrud, C., Andresen, T., Eiken, O., Hansen, H., Janbu, A., Lippard, J., Bolås, H.N., Simmenes, T.H., Teige, G.M.G., Østmo, S., 2009. Storage of CO_2 in saline aquifers–lessons learned from 10 years of injection into the Utsira Formation in the Sleipner area. Energy Proc. 1, 1997–2004. https://doi.org/10.1016/j.egypro.2009.01.260.

Hoetz, G., Steenbrink, J., Bekkers, N., Vogelaar, A., Luthi, S., 2011. Salt-induced stress anomalies: an explanation for variations in seismic velocity and reservoir quality. Petrol. Geosci. 17, 385–396. https://doi.org/10.1144/1354-079311-002.

Holloway, S., Vincent, C.J., and Kirk, K., 2006, Industrial carbon dioxide emissions and carbon dioxide storage potential in the UK. British geological survey commercial report, CR/06/185 (NC). 57 pp.

Hustoft, S., Mienert, J., Bünz, S., Nouzé, H., 2007. High-resolution 3D-seismic data indicate focussed fluid migration pathways above polygonal fault systems of the mid-Norwegian margin. Mar. Geol. 245, 89–106. https://doi.org/10.1016/j.margeo.2007.07.004.

IPCC, 2018. Summary for Policymakers. In: Global warming of 1.5°C. An IPCC Special Report on the impacts of global warming of 1.5°C above pre-industrial levels and related global greenhouse gas emission pathways, in the context of strengthening the global response to the threat of climate change, sustainable development, and efforts to eradicate poverty [V. Masson-Delmotte, P. Zhai, H. O. Pörtner, D. Roberts, J. Skea, P.R. Shukla, A. Pirani, W. Moufouma-Okia, C. Péan, R. Pidcock, S. Connors, J. B. R. Matthews, Y. Chen, X. Zhou, M. I. Gomis, E. Lonnoy, T. Maycock, M. Tignor, T. Waterfield (eds.)].

Jones, I.F., Davison, I., 2014. Seismic imaging in and around salt bodies. Interpretation 2, SL1-SL20. doi:10.1190/int-2014-0033.1.

Kilhams, B., Stevanovic, S., Nicolai, C., 2018. The 'Buntsandstein' gas play of the Horn Graben (German and Danish offshore): dry well analysis and remaining hydrocarbon potential. Geol. Soc. 469, 169–192. https://doi.org/10.1144/sp469.5. London, Special Publications.

Kley, J., 2018. Timing and spatial patterns of Cretaceous and Cenozoic inversion in the Southern Permian Basin. Geol. Soc. 469, 19–31. https://doi.org/10.1144/SP469.12. London, Special Publications.

Kley, J., Franzke, H., Jähne, F., Krawczyk, C., Lohr, T., Reicherter, K., Scheck-Wenderoth, M., Sippel, J., Tanner, D., Van Gent, H., 2008. Strain and stress, dynamics of complex intracontinental basins: the Central European basin system, pp. 97-124.

Kley, J., Voigt, T., 2008. Late Cretaceous intraplate thrusting in central Europe: effect of Africa-Iberia-Europe convergence, not Alpine collision. Geology 36. https://doi.org/10.1130/g24930a.1.

Knopf, S., May, F., 2017. Comparing methods for the estimation of CO_2 storage capacity in saline aquifers in Germany: regional aquifer based vs. Structural trap based assessments. Energy Proc. 114, 4710–4721. https://doi.org/10.1016/j.egypro.2017.03.1605.

Kopp, A., Class, H., Helmig, R., 2009a. Investigations on CO_2 storage capacity in saline aquifers. Int. J. Greenh. Gas Con. 3, 263–276. https://doi.org/10.1016/j.ijggc.2008.10.002.

Kopp, A., Class, H., Helmig, R., 2009b. Investigations on CO_2 storage capacity in saline aquifers—Part 2: Estimation of storage capacity coefficients. Int. J. Greenh. Gas Con. 3, 277–287. https://doi.org/10.1016/j.ijggc.2008.10.001.

Korevaar, S., Dalman, R., Nelskamp, S., Atkins, S., Boter, E., Wiarda, E., Nolten, M., Beintema, K., 2023. Play 5 triassic. https://www.geodeatlas.nl/pages/play-5-triassic.

Kortekaas, M., Böker, U., van der Kooij, C., Jaarsma, B., 2018. Lower Triassic reservoir development in the northern Dutch offshore. Geol. Soc. 469, 149–168. https://doi.org/10.1144/sp469.19. London, Special Publications.

Kyrkjebø, R., Gabrielsen, R.H., Faleide, J.I., 2022. Unconformities related to the Jurassic–Cretaceous synrift–post-rift transition of the northern North Sea. J. Geol. Soc. London 161, 1–17. https://doi.org/10.1144/0016-764903-051.

Lloyd, C., Huuse, M., Barrett, B.J., Newton, A.M.W., 2021a. Regional Exploration and characterisation of CO_2 storage prospects in the Utsira-Skade Aquifer, North Viking Graben, North Sea. Earth Sci. Syst. Soc. 1 https://doi.org/10.3389/esss.2021.10041.

Lloyd, C., Huuse, M., Barrett, B.J., Newton, A.N.W., 2021b. A workflow for regional exploration of CO_2 storage sites in saline aquifers. In: TCCS-11 - Trondheim Conference on CO_2 Capture, Transport and Storage. Trondheim, Norway. SINTEF Academic Press.

Martin-Roberts, E., Scott, V., Flude, S., Johnson, G., Haszeldine, R.S., Gilfillan, S., 2021. Carbon capture and storage at the end of a lost decade. One Earth 4, 1569–1584. https://doi.org/10.1016/j.oneear.2021.10.002.

McKie, T., Williams, B., 2009. Triassic palaeogeography and fluvial dispersal across the northwest European Basins. Geol. J. 44, 711–741. https://doi.org/10.1002/gj.1201.

Michelsen, O., Nielsen, L.H., Johannessen, P.N., Andsbjerg, J., Surlyk, F., 2003. Jurassic lithostratigraphy and stratigraphic development onshore and offshore Denmark. Geol. Surv. Denmark Greenl. Bull. 1, 145–216. https://doi.org/10.34194/geusb.v1.4651.

Mohr, M., Kukla, P.A., Urai, J.L., Bresser, G., 2005. Multiphase salt tectonic evolution in NW Germany: seismic interpretation and retro-deformation. Int. J. Earth Sci. 94, 917–940. https://doi.org/10.1007/s00531-005-0039-5.

Müller, S., Arfai, J., Jaehne-Klingberg, F., Bense, F., Weniger, P., 2020. Source rocks of the German Central Graben. Mar. Pet. Geol. 113, 104–120. https://doi.org/10.1016/j.marpetgeo.2019.104120.

Müller, C.O., Reinhold, K., 2011. Geologische Charakterisierung tiefliegender Speicher- und Barrierehorizonte in Deutschland-Speicher-Kataster Deutschland. In: Müller, C., Reinhold, K. (Eds.), Geologische Charakterisierung tiefliegender Speicher- und Barrierehorizonte in Deutschland – Speicher-Kataster Deutschland. – Schriftenreihe der Deutschen Gesellschaft für Geowissenschaften. Schweizerbart, Hannover, pp. 9–27.

Müller, S., Reinhardt, L., Franke, D., Gaedicke, C., Winsemann, J., 2018. Shallow gas accumulations in the German North Sea. Mar. Pet. Geol. 91, 139–151. https://doi.org/10.1016/j.marpetgeo.2017.12.016.

Müller, S.M., Jähne-Klingberg, F., Thöle, H., Jakobsen, F.C., Bense, F., Winsemann, J., Gaedicke, C., 2023. Jurassic to lower Cretaceous tectonostratigraphy of the German Central Graben, southern North Sea. Neth. J. Geosci. 102 https://doi.org/10.1017/njg.2023.4.

Nilsen, H.M., Lie, K.-A., Møyner, O., Andersen, O., 2015. Spill-point analysis and structural trapping capacity in saline aquifers using MRST-CO_2lab. Comput. Geosci. 75, 33–43. https://doi.org/10.1016/j.cageo.2014.11.002.

NLOG, 2023. Dutch Oil andGas Portal, http://www.nlog.nl.

Olivarius, M., Weibel, R., Friis, H., Boldreel, L.O., Keulen, N., Thomsen, T.B., 2017. Provenance of the lower Triassic bunter sandstone Formation: implications for distribution and architecture of aeolian vs. fluvial reservoirs in the North German Basin. Basin Res. 29, 113–130. https://doi.org/10.1111/bre.12140.

Olivarius, M., Weibel, R., Hjuler, M.L., Kristensen, L., Mathiesen, A., Nielsen, L.H., Kjøller, C., 2015. Diagenetic effects on porosity–permeability relationships in red beds of the lower Triassic bunter sandstone formation in the North German Basin. Sediment. Geol. 321, 139–153. https://doi.org/10.1016/j.sedgeo.2015.03.003.

Patruno, S., Green, A., Corcoran, J., Caldarella, D., Scisciani, V., Przywara, M., 2024. A conceptual CO_2 fill-and-spill mega-fairway in the UK Southern North Sea: a new approach to identify and optimise large-scale underground carbon storage (CCS). Int. J. Greenh. Gas Con. 133, 104092 https://doi.org/10.1016/j.ijggc.2024.104092.

Peeters, S., Asschert, A., Verweij, H., 2018. Towards a better understanding of the highly overpressured lower Triassic bunter reservoir rocks in the Terschelling basin. Geol. Soc. 469, 223–236. https://doi.org/10.1144/sp469.13. London, Special Publications.

Pharaoh, T.C., Dusar, M., Geluk, M.C., Kockel, F., Krawczyk, C.M., Krzywiec, P., Scheck-Wenderoth, M., Thybo, H., Vejbæk, O.V., Van Wees, J.D., 2010. Tectonic evolution. In: Doornenbal, J.C., Stevenson, A.G. (Eds.), Petroleum Geological Atlas of the Southern Permian Basin Area. EAGE Publications b.v, Houten, pp. 25–57.

Röhling, H.G., 1991. A lithostratigraphic subdivision of the lower Triassic in the northwest German lowlands and the German sector of the North Sea, based on gamma-ray and sonic logs. Geol. Jahrb. A 3–24.

Rutqvist, J., 2012. The Geomechanics of CO_2 storage in deep sedimentary formations. Geotech. Geol. Eng. (Dordr) 30, 525–551. https://doi.org/10.1007/s10706-011-9491-0.

Schäfer, F., Walter, L., Class, H., Müller, C., 2012. The regional pressure impact of CO_2 storage: a showcase study from the North German Basin. Environ. Earth Sci. 65, 2037–2049. https://doi.org/10.1007/s12665-011-1184-8.

Span, R., Wagner, W., 1996. A new equation of state for carbon dioxide covering the fluid region from the triple-point temperature to 1100 K at pressures up to 800 MPa. J. Phys. Chem. Ref. Data 25, 1509–1596.

Thöle, H., Bense, F., Stück, H., Jähne-Klingberg, F., 2022. Potenziale des unterirdischen Speicher- und Wirtschaftsraumes im Norddeutschen Becken (TUNB) – Abschlussbericht Teilprojekt 6: 3D-Strukturmodell Deutsche Nordsee. Bundes. Geowissen. Rohstoffe (BGR), Hannover 112.

Thöle, H., Jähne-Klingberg, F., Doornbell, H., den Dulk, M., Britze, P., Jakobsen, F., 2021. Harmonized depth models and structural framework of the NL-GER-DK North Sea, GEOERA 3DGEO-EU 3D Geomodeling for Europe - Project number: GeoE.171.005.

Thöle, H., Jähne-Klingberg, F., Doornenbal, H., den Dulk, M., Britzke, P., Jakobsen, F., 2020. Harmonized seismic stratigraphic concepts - A base for consistent structural interpretations, 3DGEO-EU: 3D Geomodeling for Europe - Project number: GeoE.171.005.

Tillner, E., Kempka, T., Nakaten, B., Kühn, M., 2013. Brine migration through fault zones: 3D numerical simulations for a prospective CO_2 storage site in Northeast Germany. Int. J. Greenh. Gas Con. 19, 689–703. https://doi.org/10.1016/j.ijggc.2013.03.012.

Tucker, M.E., 1991. Sequence stratigraphy of carbonate-evaporite basins: models and application to the Upper Permian (Zechstein) of northeast England and adjoining North Sea. J. Geol. Soc. London 148, 1019–1036. https://doi.org/10.1144/gsjgs.148.6.1019.

Underhill, J.R., Partington, M., 1993. Jurassic thermal doming and deflation in the North Sea: implications of the sequence stratigraphic evidence. Geol. Soc. 337–345. https://doi.org/10.1144/0040337. London, Petroleum Geology Conference Series. The Geological Society of London.

V. Gessel, S., Hintersberger, E.V. Ede, R., ten Veen, J., Doornenbal, H., Diepolder, G.W., den Dulk, M., Hamiti, S., Vukzaj, N., Çako, R., Prendi, E., Ceroni, M., Mara, A., Barros, R., Tovar, A., Britze, P., Baudin, T., Stück, H., Jähne-Klingberg, F., Jahnke, C., Höding, T., Malz, A., Kristjánsdóttir, S., Þorbergsson, A., Di Manna, P., D'Ambrogi, C., Congi, M., Lazauskienė, J., Andriuškevičienė, G., Baliukevičius, A., Jarosiński, M., Gogołek, T., Stępień, U., Krzemińska, E., Salwa, S., Habryn, R., Aleksandrowski, P., Szynkaruk, E., Konieczyńska, M., Ressurreição, R., Machado, S., Moniz, C., Sampaio, J., Dias, R., Carvalho, J., Fernandes, J., Ramalho, E., Filipe, A., Celarc, B., Atanackov, J., Jamšek Rupnik, P., Shevchenko, A., Melnyk, I., and Lapshyna, A., 2021, The HIKE European fault database (EFDB) compiled in the framework of the GeoERA project HIKE. https://geoera.eu/projects/hike10/faultdatabase/.

van der Molen, A.S., 2004. Sedimentary development, seismic stratigraphy and burial compaction of the Chalk Group in the Netherlands North Sea area. PhD Thesis. Univeristy Utrecht.

van der Molen, A.S., Dudok van Heel, H.W., Wong, T.E., 2005. The influence of tectonic regime on chalk deposition: examples of the sedimentary development and 3D-seismic stratigraphy of the Chalk Group in the Netherlands offshore area. Basin Res. 17, 63–81. https://doi.org/10.1111/j.1365-2117.2005.00261.x.

van Kempen, B.M.M., Mijnlieff, H.F., van der Molen, J., 2018. Data mining in the Dutch oil and gas portal: a case study on the reservoir properties of the Volpriehausen Sandstone interval. Geol. Soc. 469, 253–267. https://doi.org/10.1144/sp469.15. London, Special Publications.

van Wees, J.D., Stephenson, R.A., Ziegler, P.A., Bayer, U., McCann, T., Dadlez, R., Gaupp, R., Narkiewicz, M., Bitzer, F., Scheck, M., 2000. On the origin of the Southern Permian Basin, Central Europe. Mar. Petrol. Geol. 17, 43–59. https://doi.org/10.1016/s0264-8172(99)00052-5.

Vangkilde-Pedersen, T., Anthonsen, K.L., Smith, N., Kirk, K., van der Meer, B., Le Gallo, Y., Bossie-Codreanu, D., Wojcicki, A., Le Nindre, Y.-M., Hendriks, C., Dalhoff, F., Christensen, N.P., 2009. Assessing European capacity for geological storage of carbon dioxide–the EU GeoCapacity project. Energy Proc. 1, 2663–2670. https://doi.org/10.1016/j.egypro.2009.02.034.

Ward, N.I.P., Alves, T.M., Blenkinsop, T.G., 2016. Reservoir leakage along concentric faults in the Southern North Sea: implications for the deployment of CCS and EOR techniques. Tectonophysics 690, 97–116. https://doi.org/10.1016/j.tecto.2016.07.027.

Warsitzka, M., Jähne-Klingberg, F., Kley, J., Kukowski, N., 2018. The timing of salt structure growth in the Southern Permian Basin (Central Europe) and implications for basin dynamics. Basin Res. 31, 337–360. https://doi.org/10.1111/bre.12323.

Wellmann, J.F., Horowitz, F.G., Schill, E., Regenauer-Lieb, K., 2010. Towards incorporating uncertainty of structural data in 3D geological inversion. Tectonophysics 490, 141–151. https://doi.org/10.1016/j.tecto.2010.04.022.

White, J.A., Foxall, W., 2014. A Phased approach to induced seismicity risk management. Energy Proc. 63, 4841–4849. https://doi.org/10.1016/j.egypro.2014.11.515.

Wilson, M., Neumann, E.R., Davies, G.R., Timmerman, M.J., Heeremans, M., Larsen, B. T., 2004. Permo-Carboniferous magmatism and rifting in Europe: introduction. Geol. Soc. 223, 1–10. https://doi.org/10.1144/gsl.Sp.2004.223.01.01. London, Special Publications.

Wolf, M., Steuer, S., Röhling, H.-G., Rebscher, D., Jähne-Klingberg, F., 2015. Lithofacies distribution in the Central European Basin: a 3D model of the Buntsandstein facies in the central German North Sea. Zeitschrift Deutschen Gesellschaft Geowissenschaften 166, 341–359. https://doi.org/10.1127/zdgg/2015/0039.

Wu, L., Thorsen, R., Ottesen, S., Meneguolo, R., Hartvedt, K., Ringrose, P., Nazarian, B., 2021. Significance of fault seal in assessing CO_2 storage capacity and containment risks – an example from the Horda Platform, northern North Sea. Petrol. Geosci. 27. https://doi.org/10.1144/petgeo2020-102.

Zhou, Q., Birkholzer, J.T., 2011. On scale and magnitude of pressure build-up induced by large-scale geologic storage of CO_2. Greenh Gas.: Sci. Technol. 1, 11–20.

Zhou, Q., Birkholzer, J.T., Tsang, C.-F., Rutqvist, J., 2008. A method for quick assessment of CO_2 storage capacity in closed and semi-closed saline formations. Int. J. Greenh. Gas Con. 2, 626–639. https://doi.org/10.1016/j.ijggc.2008.02.004.

Ziegler, P.A., 1990. Geological Atlas of Western and Central Europe, 2nd edition. Geological Society Publishing House (Bath), Shell Internationale Petroleum Maatschappij.